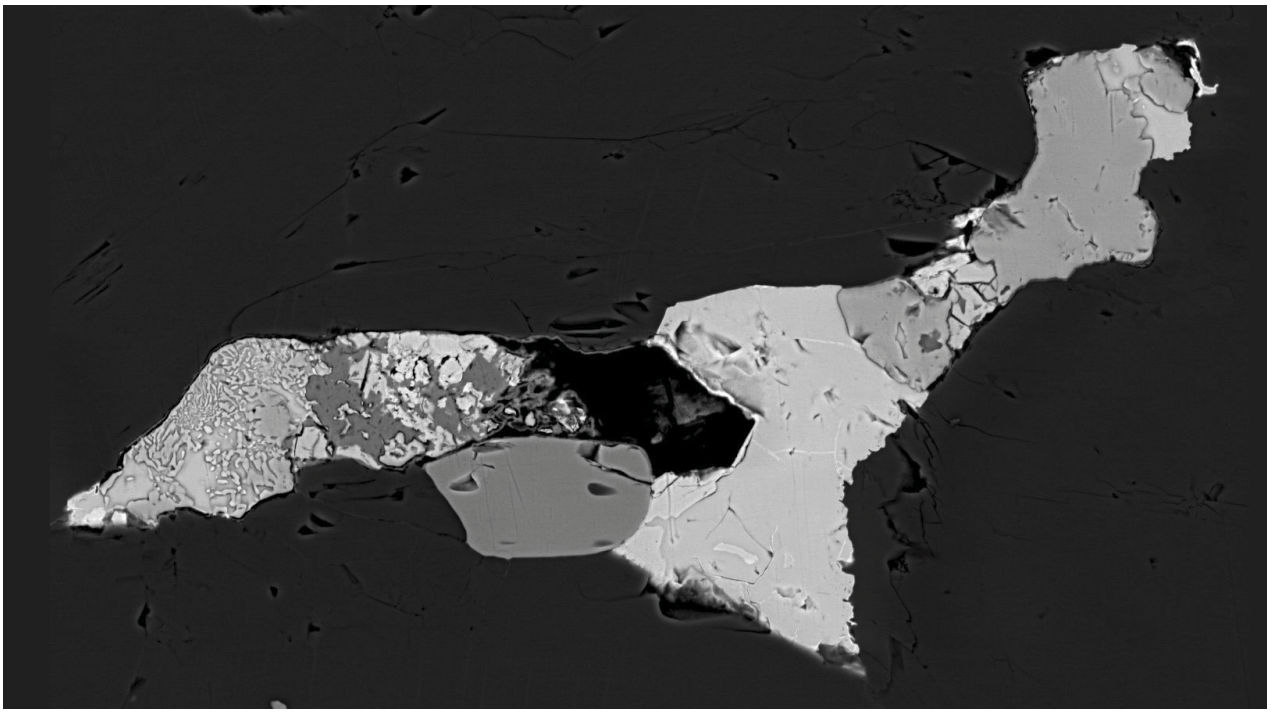
Stockholm University

Master Thesis

Degree Project in
Geology 30 hp

Mineral hosts for gold in an Archean greenstone belt: The La Grande Greenstone Belt, Canada

Manuel Naveiras Villamea



Stockholm 2024

Department of Geological Sciences
Stockholm University
SE-106 91 Stockholm

CONTENTS

Abstract

Abbreviations

1. Theoretical Background 4
2. Geological Setting 7
3. Samples 8
4. Methods 11
5. Results 12
6. Discussion 24
7. Conclusion 30
8. References 32

Abstract:

This study investigates the mechanisms of gold depletion in metabasaltic rocks within the La Grande Subprovince, Canada, during prograde metamorphism. Previous studies have highlighted metasedimentary rocks as sources of gold, with the pyrite-pyrrhotite transformation identified as a key process in gold liberation. Metabasaltic terrains, abundant in greenstone belts, exhibit similar progressive gold depletion as the metamorphic grade increases. This research builds upon earlier work by studying the mechanisms of gold depletion in metabasalts with a combination of ore microscopy, Scanning Electron Microscopy (SEM), and Laser Ablation Inductively Coupled Plasma Mass Spectrometry (LA-ICP-MS) to analyse the sulfide mineral phases and their gold content across varying metamorphic grades. The analytical results identify pyrite and pyrrhotite as important gold hosts in the low metamorphic conditions and confirms their gold content decrease along metamorphism. Chalcopyrite is identified as a refractory repository of gold. The mineralogical and textural interpretation of the petrographic study of the sections has been used to build a suitable framework for the metabasaltic rocks, that draws a scene with various potential paragenetic succession converging on a pervasive retrogression, particularly intense in the high metamorphic grade groups, that partially obscures the clear identification of the processes responsible for gold depletion. Nonetheless, the study suggests that the prograde transformation of pyrite into pyrrhotite may also be a contributing factor in the gold depletion of metabasalts, and simultaneously, identifies potential space for other mechanisms beyond sulfide phase transformation involved in this gold depletion.

Key words: Orogenic Gold Deposits, Metabasaltic Rocks, Sulfide Paragenesis, Gold Depletion, Laser Ablation ICP-MS, Gold Mobilization

Abbreviations

Ccp – Chalcopyrite

Py – Pyrite

Po – Pyrrhotite

Pn – Pentlandite

Mll – Millerite

Mol – Molybdenite

Mt – Magnetite

Cv – Covellite

Cb – Cobaltite

Sp – Sphalerite

Ilm – Ilmenite

ISS – Intermediate Solid Solution

MSS – Monosulfide Solid Solution

LA-ICP-MS – Laser Ablation - Induced Coupled Plasma - Mass Spectrometry

SEM-EDS – Scanning Electron Microscopy - Energy Dispersive Spectroscopy

FeOx – Iron Oxide

1. THEORETICAL BACKGROUND

1.1. Introduction

Understanding the sources of gold for orogenic systems plays a major role in assessing regional prospectivity and can provide guidance for mineral exploration and the economic geology field. Orogenic gold deposits are significant contributors to global gold production, providing up to 50% of the world's historical gold production, including the secondary placer deposits derived from them (Frimmel, 2008). These deposits form in compressional settings associated with crustal thickening and prograde metamorphism. In recent literature, after the development of methods for the ultra-low detection limit quantification of gold in potential source rocks (Pitcairn et al., 2006b), metasediments and metabasalts have been indicated as potential sources of gold. Gold is progressively depleted in these rocks during metamorphism, and this feature that has been observed in multiple different orogens (Patten et al., 2020). The mineralogical controls involved in the liberation of gold during metamorphism are, in the case of metasedimentary rocks, reasonably well understood with the pyrite pyrrhotite transition playing a central role (Pitcairn et al., 2016). This thesis focuses on the mechanisms underlying gold liberation in metabasaltic rocks which has until now not been investigated.

This work is based on a suite of metabasaltic rock samples from upper greenschist to upper amphibolitic metamorphic conditions from La Grande Subprovince, Canada, that have been previously reported to show depletion of gold with increasing metamorphic grade (Patten et al., 2020). Greenstone belts, such as La Grande, are significant hosts of orogenic gold deposits. Recent studies have shown that metabasalts which are much more abundant than metasedimentary rocks within these belts, also liberate gold during metamorphism, but the mineral reactions responsible are not well understood. La Grande greenstone belt showing a clear metamorphic transition in metavolcanic rocks, making it a prime location to study these processes, offering the conditions to research the mechanism of gold mobilisation.

This study aims to identify the mineralogical hosts for gold in the metabasaltic rocks from the La Grande subprovince and investigate the mechanisms that have contributed to the decreasing gold content during metamorphism. The samples in this study have been previously characterised into 3 groups of different metamorphic conditions (Peillod, A., 2019). This study employs a combination of ore microscopy and Scanning Electron Microscopy to characterise and quantify the sulfide phases present in these groups. Subsequently, Laser Ablation Inductively Coupled Plasma Mass Spectrometry has been used to measure gold concentrations within the different sulfide grains. Integration of sulfide abundances and in situ Au contents in sulfide minerals, with the whole rock Au content allows an approximation for the allocation of the gold inventory in its main hosts. The initial hypothesis that is guiding the strategy to face the aim of the study is based on previous studies on sedimentary rocks, where the prograde transition of pyrite into pyrrhotite appears as responsible for the liberation of gold (Pitcairn et al., 2016). However, a more complex framework has to be developed for the evolution of the magmatic systems and its gold content through its metamorphic path.

1.2. Archean orogenic gold deposits and greenstone belts

In general terms, an orogenic gold deposit can be defined as a structurally hosted deposit that occurs in an orogenic belt. These gold deposits are formed in compressional or transpressional settings, associated with the crustal thickening and prograde metamorphism. They have been preferentially formed in the three main time periods related to tectonic convergence and crustal growth; the Archean around 2.7 Ga, the Paleoproterozoic around 1.9 Ga and the Paleozoic (Goldfarb et al., 2001).

Archean orogenic gold deposits occur within granite-greenstone belts such as the Superior Craton, Canada or the Yilgarn Craton, Australia. These volcanic formations are usually more sensitive to deformation than the felsic block surrounding them, and they tend to form weak structural zones favourable for fluid paths, which are also chemically favourable for trapping the fluids producing the metal deposition. As a result, the structurally hosted orogenic deposits tend to occur in 2nd and 3rd order faults associated with these major crustal discontinuities, frequently associated with terrain boundaries. The gold deposits can nonetheless be hosted by many lithologies associated with these greenstone belts, such as mafic and ultramafic, metasediments and even felsic rocks. These deposits generally show high-strain features close to the brittle-ductile transition, indicating the fundamental structural control of the mineralisation.

1.3. Sources of fluids and metals

The study of the sources of fluids and metals significantly impacts the prospectivity modelling of fertile regions. Different sources for the fluids and metals have been discussed in the literature, including fluid exsolution from magmatic rocks, fluid input through trans-crustal faults, or metamorphism and devolatilisation of the crust (Goldfarb, 2015). Leaving aside cases in which several of these mechanisms could come together, the metamorphic option has gathered substantial evidence from the geological, geochemical and geochronological studies. This evidence suggests that most significant orogenic gold deposits are formed through metamorphic rather than magmatic-hydrothermal processes (Goldfarb, 2023). Some geochemical characteristics of a particular deposit can indicate its source material: metasedimentary rocks are likely to be essential sources of Au and the main source of As, Sb and S; magmatic-hydrothermal fluids may be important local sources of metals in deposits enriched in Mo, Bi and Te; and deposits formed from predominantly metavolcanic source rock have much higher Au/As than deposits formed from metasedimentary source rocks (Pitcairn et al., 2017). The metamorphic devolatilization of large volumes of rock seems to be the driving factor of fluid generation. The breakdown of chlorite in biotite to staurolite-zone can release up to 1% of the total weight of the metamorphosed rock mass of water (Piette-Lauzière et al., 2019). The gold added to these metamorphic fluids is incorporated in the devolatilisation scenario and not in further leaching of rocks along the fluid transport (Phillips & Powell, 2010). The pyrite-pyrrhotite transition has been identified as the responsible transformation releasing gold into the fluids in metasedimentary sources during prograde metamorphism (Pitcairn et al., 2006a; Tomkins, 2010), and it is suspected to be involved in the case of metabasaltic terrains (Patten et al., 2020).

1.4. Role of Metabasalts

Metabasalts can play a significant metallogenetic role by liberating its gold component during metamorphism, as they constitute one of the most abundant supracrustal rocks. Figure 1 shows how different metavolcanic sequences from La Grande subprovince in Canada and the Central Lapland Greenstone Belt (CLGB) in Finland get progressively depleted in gold as the metamorphic grade increases. This evidence has been applied to estimate the prospectivity of the Finnish belt based on the estimation of the basaltic volumes that have reached amphibolitic facies. Patten et al. (2023) conclude that up to 2500 t of Au could have been liberated in the CLGB by these metamorphism, which represent one order of magnitude greater than the reported Au resources in the area. These values are consistent with the estimations of undiscovered gold resources in this belt (Niiranen et al., 2015). Important recent gold discoveries, such as the 131 t Au Ikkari gold deposit, located 2km south of the base of the Kittilä block, could provide new evidence for this metamorphic model, as the high Au/As ratios of the mineralisation are the expected ones from a metabasaltic rather than metasedimentary source (Pitcairn et al., 2017).

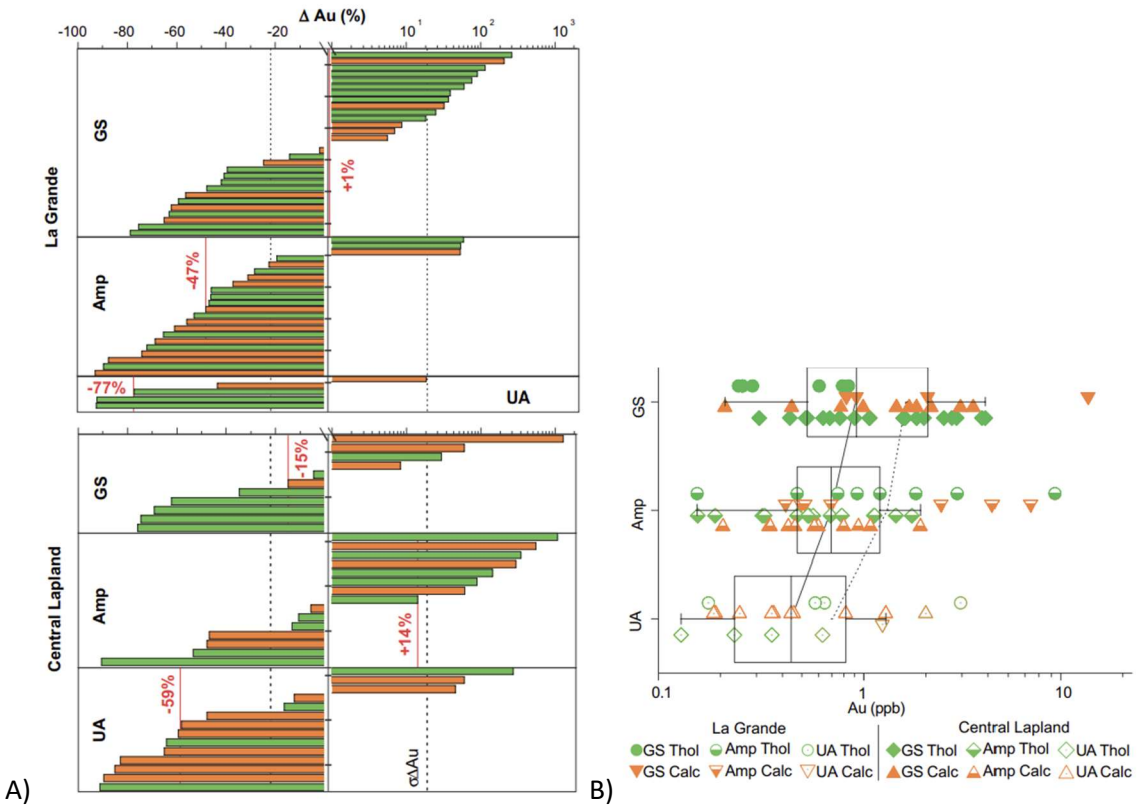


Figure 1 A) Au mass variation in the La Grande Subprovince and the Central Lapland Greenstone Belt. Orange bars indicate tholeiitic affinity, and green, calc-alkaline. Red values are median mass variations. σΔAu (mass variation uncertainty in dotted lines). GS-Greenschist facies, Amp-Amphibolitic facies, US-Upper amphibolite facies. B) Au content in metavolcanic rocks from La Grande and Central Lapland Greenstone Belt by metamorphic facies. The solid curve connects the median values of each group, and the dashed curve connects the average values. Box ranges are defined by 25th and 75th percentiles, and the whiskers by the lower and inner fence, both from Patten et al. 2023.

2. GEOLOGICAL SETTING

Greenstone belts in Archean and Proterozoic cratons are well-known metallogenic districts around the globe. The La Grande subprovince, situated within the east-central sector of the Superior Province, Canada (Fig 1), constitutes a greenstone belt containing metamorphosed volcanic and minor sedimentary rocks and dominantly granitoid intrusive rocks. The two foremost submarine volcanic assemblages, the Guyer Group (2820-2806 Ma) and the Yasinski Group (2751-2732 Ma) (Goutier et al., 2003; David et al., 2012), are disaggregated into lenses and enclosed by sedimentary siliciclastic sequences of the Apple formation, with minimal detrital zircon ages of 2750 Ma, that are overlaying the tonalitic Mesoarchean basement, dating from 3452 to 2788 Ma (Davis et al., 2014). Intermediate to felsic plutonic rocks intruded these formations at 2716-2709 Ma (Mercier-Langevin et al., 2012).

The presence of rift-related volcanic rocks is interpreted as a failed rifting episode (Sappin et al. 2018). Several pillow lavas occurrences in the region are indicative of these attempts of early aborted oceanic crust formation. These conditions are indicative a hot mantle and a thin crust in the Neoarchean. However, actual crustal thickness estimations indicate a regional thickening toward the La Grande belt. The main magmatic and metamorphic events in the Superior Province overlap in time. As the regional settings changed from the extensional proto-rifting to the compressional scenario, the central-eastern Rivière Arnaud terrane collided with the western continental block of Hudson Bay, driving high-grade Barrovian metamorphism at 2700 M during the accretion. Later, lower pressure and higher temperature metamorphism will overprint the basaltic formations (Percival et al., 2012).

Structurally, the La Grande subprovince exhibits a prominent east-northeast trending foliation, indicating a substantial tectonic imprint on the region. The geological evolution of La Grande has been marked by four major Archean compressional deformation events and three associated metamorphic episodes, as exposed by Goutier et al., 2003. These complex geological processes have intricately shaped the fabric of the rocks in the area, making them a focus for mineral exploration. The Roberto gold deposit, currently mined at the Éléonore operation, is a significant example of the region's potential, with an estimated resource of approximately 8.8 million ounces of gold (Fontaine et al., 2017). Beyond Roberto, the La Grande hosts various gold and base metal mineral deposits, conferring economic and strategic importance to the area.

3. SAMPLES

An original suite of 90 samples was previously collected from 41 locations in the La Grande area. After the exclusion of weathered, volcanoclastic, and mineralised samples, 80 samples from the Yasinski, Guyer and La Forge groups were selected for the study (Figure 2). The samples were collected in 2017 and have undergone petrographic investigation and lithogeochemical analyses prior to this thesis. The petrographic investigation of silicate mineral phases was carried out by Alexander Peilloid in 2019, in order to constrain the metamorphic conditions. This work is yet unpublished and is referred to here as Peillod, 2019. Some of the lithogeochemical data is published in Patten et al. (2020) but is otherwise unpublished.

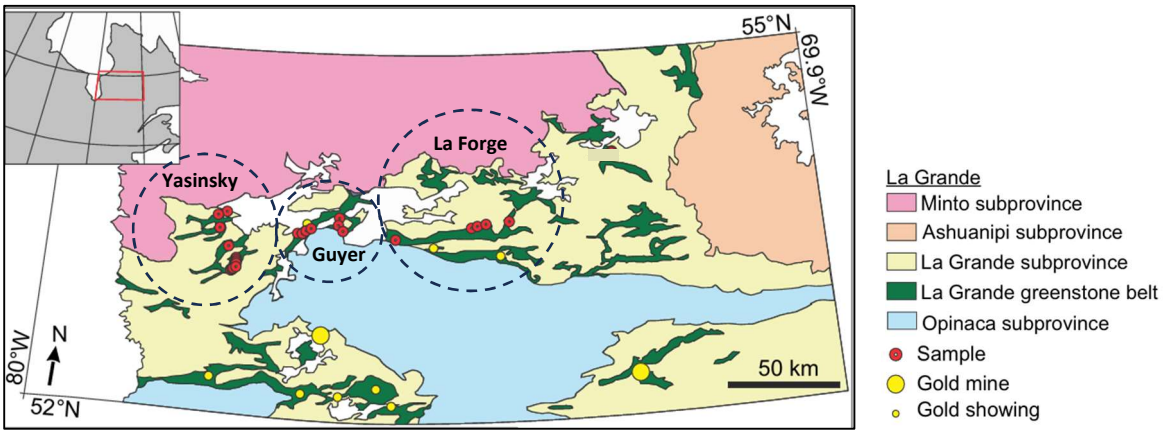


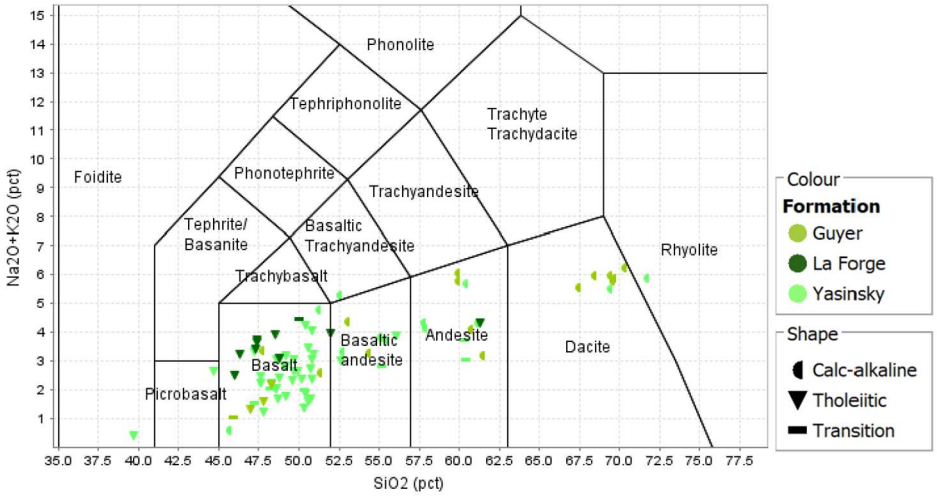
Figure 2. The geological map of La Grande Subprovince shows sample locations in the Yasinsky, Lac Guyer, And Riviere-La Forge areas. Modified after Patten et al., 2020.

The metavolcanic rocks of the Yasinsky unit proceed from the western parts of the La Grande area, and its samples comprise a total of 54 upper greenschist-lower amphibolitic facies samples. As the regional metamorphic grade increases towards the East, the Yasinsky metabasalts represent the lowest metamorphic grade of the set of samples. In these samples, the magmatic assemblage (Mg-hornblende with symplectite, andesine, alkali-feldspar, and ilmenite) can still be observed, and the metamorphic blasts do not yet reach 1mm size, being smaller than those in Guyer and La Forge. The metamorphic overprint includes prograde and retrograde phases such as actinolite, albite, chlorite and titanite with minor epidote.

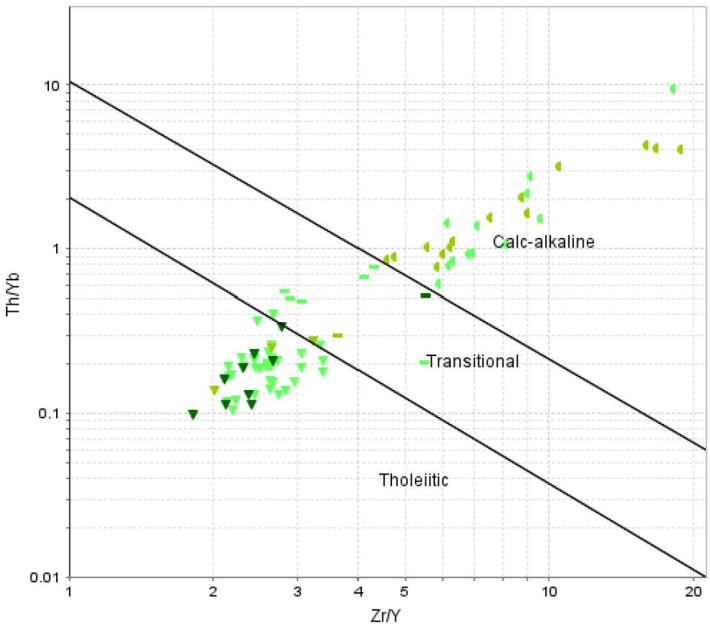
The samples from the Guyer unit represent the metavolcanic of intermediate metamorphic grade of the collection, with all its 18 samples representing amphibolite facies. These metabasalts of calc-alkaline affinity experienced metamorphism at amphibolite to upper amphibolite facies. The general composition of these rocks is magnesio-hornblende amphibole, andesitic plagioclase (An_{45-51}), biotite, ilmenite, and locally pyroxene and anorthoclase (Or_{13-33}; An_{8-10}). Later, greenschist metamorphism overprints the samples, with chlorite replacing biotite and hornblende and advanced sericitisation of the plagioclase and alkali feldspar.

Finally, the 10 metabasaltic samples from the La Forge unit exhibit mineral assemblages from the highest metamorphic grade at upper amphibolite facies, with no evidence of the primary magmatic phases. The major constituents of these rocks are amphibole of magnesio-hornblende and tchermakitic composition, oligoclase (An_{25-32}), orthoclase (Or_{90-100}), biotite, ilmenite, and occasional garnet and rutile.

The estimations of the metamorphic temperatures have been carried out based on semi-quantitative SEM mineral compositions applied to plagioclase-hornblende and Ti-in-biotite thermometry and Al-in-hornblende barometry (Peilloid, 2019). In the Yasinsky samples, the metamorphic amphibole and plagioclase offer a range of 480-530 ± 40°C at pressures of 1 ± 0.7 kbar. Measurements of Ti-in-biotite thermometry support that range, pointing to a temperature around 500°C. The samples from Guyer show plagioclase-hornblende thermometry and Al-in-hornblende barometry give P-T conditions for amphibolite facies metamorphism at 630-700°C and 1-6 kbar. Finally, the samples from La Forge present, with the same methods, metamorphic conditions of 700-750 ± 40°C at 7-8 ± 0.7 kbar.



A)



B)

Figure 3. A) TAS classification of the samples after Le Maitre, 1989. B) Magmatic affinity of volcanic rocks based on trace element ratios, after Ross and Bedard, 2009.

The samples can be classified in the TAS diagrams based on their whole rock composition as a mafic set ranging from basalts, basaltic andesites, andesites and dacites, with a representation of one foidite, one picrobasalt, one basaltic trachyandesite and one rhyolite (Figure 3 Figure 3. A). The samples show different affinities, grouping in the Th/Yb vs Zr/Y diagram as a tholeiitic series (n=34) and a Calc-alkaline one (n=25). Both the Yasinsky and Guyer groups show a mixture between calc-alkaline and tholeiitic compositions. The La Forge group shows tholeiitic composition (Fig. 3b). The

sample set exhibits a generalised pristine composition, after the exclusion of altered or mineralised exemplars.

The whole rock gold content of the sample set was analysed using the ultra-low detection limit method described by Pitcairn et al. (2006). It ranges from a maximum of 3.81 ppb in the low metamorphic grade Yasinski sample LG 38 to a minimum of 0.13 ppb in the high metamorphic grade La Forge sample LG 54. When trace element content is plotted against the metamorphic temperature grouping (Figure 4), progressive depletion of LOI, a proxy for H20, C, Au, As, and light depletion of Cu and Sb can be observed as the metamorphic grade increases. Other trace contents, such as Se, Bi, Te, Ni, or Co, do not appear to be affected by the metamorphic grade.

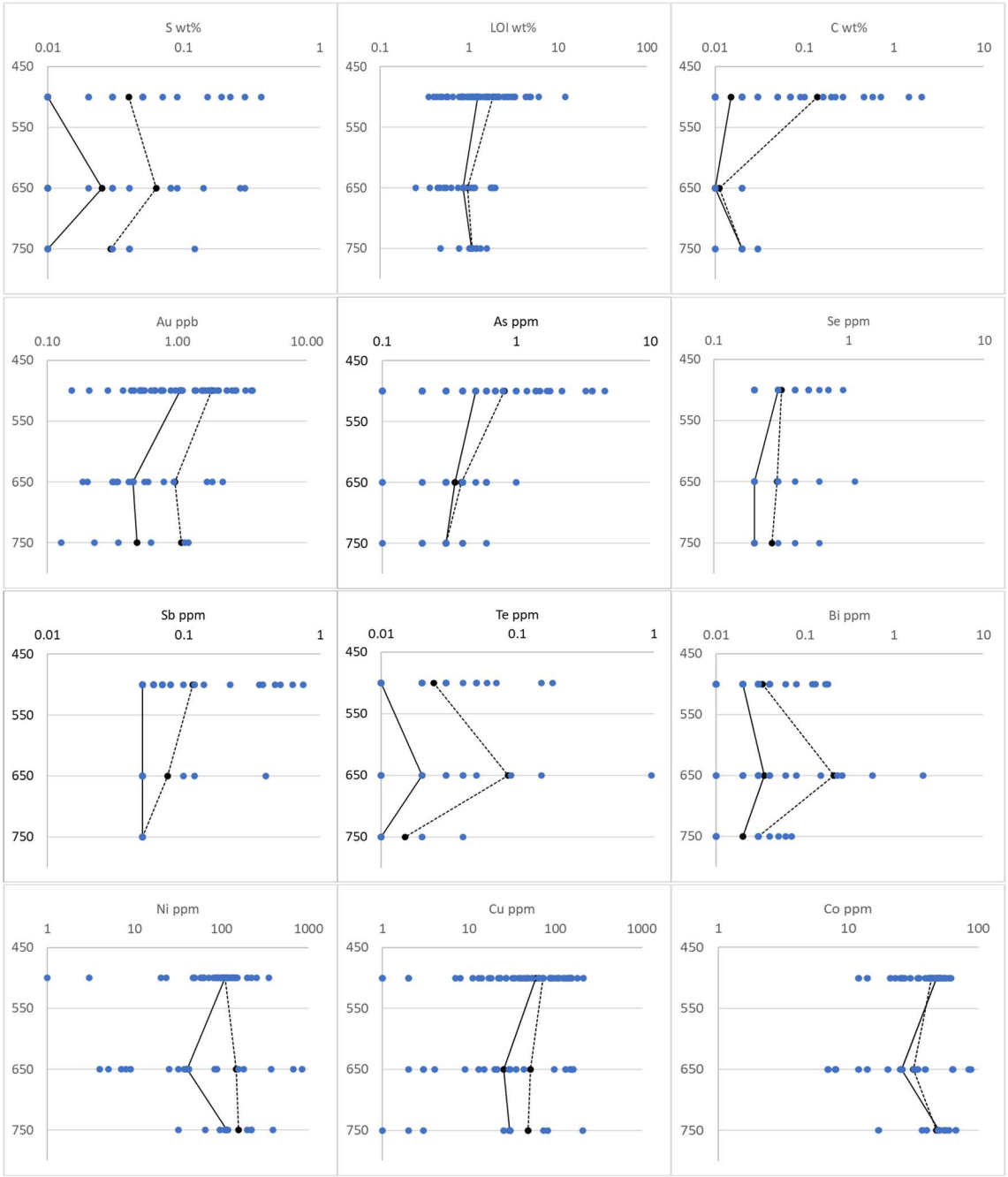


Figure 4. Whole rock trace content evolution of the metabasaltic set vs metamorphic grade. The solid curve connects the median values of each group, and the dashed curve connects the average values.

4. METHODS

From the original set of 90 samples, 88 were assayed for major and trace elements by ALS Global prior to this work. Au was analysed at Stockholm University following the ultra-low detection limit method of Pitcairn et al. (2006b), which provides a 3s detection limit of 0.02 ppb.

A selection of 48 thin sections and 12 thick sections representing the different metamorphic groups have been used to characterise the sulfide speciation and their relative proportion using reflected light microscopes at the University of Stockholm. Eighteen of these samples have been studied using a Quanta FEG 650 scanning electron microscope (SEM) at the Swedish Museum of Natural History (NRM). Prior to chemical analyses, samples were coated with 15nm of carbon. The instrument is fitted with an 80mm2 Oxford Instruments Energy Dispersive X-ray Spectrometer (EDS), which was used for semi-quantitative chemical analysis of minerals. Analytical conditions were 20 kV beam, beam size > 1 µm, working distance 10 mm. The electron beam current was calibrated prior to analysis on a cobalt metal standard, which in turn was calibrated against metal and mineral standards for each element. 10 thick sections and two thin sections were finally selected for the laser ablation ICP analyses.

ICP-MS-LA analysis

The trace compositions of the sulfide grains were obtained by in situ Laser Ablation Inductively Coupled Plasma Mass Spectrometry at the Department of Earth Sciences of the University of Gothenburg using an Agilent 8800QQQ triple Quadrupole ICP-MS coupled to a New Wave NWR 213 laser ablation system. A total of 220 points were analysed, with spot sizes of 12 to 15 μm. The laser pulse frequency was set to 10 Hz, and the laser energy density was set to 5.5 J/cm^2 for the sulfide analyses. The spot analysis was run after 15 seconds of background signal acquisition, 35 seconds of ablation and 22 seconds of wash-out. The standardisation was conducted using four reference materials: the silicate glasses NIST-SRM-610 (Jochum et al., 2011) and BCR-2G (Jochum et al., 2005), the polymetallic sulfide pellet Mass-1 (Wilson et al., 2002) and the synthetic pyrrhotite Po-725 (Sylvester et al., 2005). The reference materials were grouped in silicate sulfide pairs and alternatively analysed after every 10 sample analyses. The signal of the following isotopes was monitored: ^{24}Mg, ^{27}Al, ^{28}Si, ^{32}S, ^{44}Ca, ^{48}Ti, ^{56}Ti, ^{59}CO, ^{60}Ni, ^{63}Cu, ^{66}Zn, ^{75}As, ^{80}Se, ^{105}Pd, ^{107}Ag, ^{121}Sb, ^{125}Te, ^{128}Te, ^{181}Ta, ^{197}Au, ^{208}Pb, and ^{209}Bi. The calibration was performed with Glitter software, using ^{56}Fe as an internal standard, as derived from the stoichiometry of the analysed mineral phases. The 20 gold values obtained from the measurement of NISTSRM610 offer an average of 23.75 µg/g, which aligns with the range of 22.5 - 25 µg/g recorded in the publicly accessible measurements database (GeoReM, 2024).

5. RESULTS

5.1. Sulfide Characterization

The relative sulfide characterisation and quantification elaborated in ore microscopy and SEM-EDS are collected in Table 1. Whole rock S values provide an estimation of the sulfide mass in the sample, and the Au Whole rock value indicates the degree of Au depletion. The very fine grain size of most of the accessory sulfides made their identification only possible at the electronic microscope stage, so their characterisation is not exhaustive.

	Thin section	Whole Rock Au (ppb)	Whole Rock S (wt %)	Py	Po	Ccp	Others	SEM-EDS	LA-ICP-MS
Yasinsky 480-530 ± 40°C	LG02	0.67	0.05	29	48	23		X	X
	LG03	1.40	0.01	60	20	20			
	LG04	0.54	0.03	73	25	2	Pn, Mol	X	
	LG07	0.15	0.01	100					
	LG10	0.47	0.01	85		15	Cv, Cb	X	X
	LG 13	0.63	0.01	98		2			
	LG 14	0.79	0.01			100			
	LG 17	1.58	0.01	99		1			
	LG 19	3.72	0.05	94		6			
	LG 21	2.42	0.09	98		2	Mll, Bornite	X	X
	LG 22	1.05	0.22	98		2			
	LG 23	0.29	0.07	1	94	5	Pn	X	X
	LG 26	0.75	0.03	80	7	13			
	LG 27	0.75	0.37	97		3	Sp, Galena	X	X
	LG 28	3.35	0.01	2		98			
	LG 31	0.52	0.01			100			
	LG 32	2.78	0.02	51	22	27	Mll, Sp	X	X
	LG 33	1.65	0.01	50		50	Sp	X	
	LG 34	0.21	0.01	100					
	LG 36	0.89	0.01	5	45	50			
	LG 37	2.08	0.01	5		95			
	LG 38	3.81	0.01			100			
	LG 39	2.86	0.01				Mol	X	
	LG 41	2.06	0.01	20		80			
	LG 44	0.44	0.02	97		3			
	LG 48	0.38	0.01	25		75			
	LG 49	1.94	0.01	71		29			
	LG86	0.53	0.01	1		99	4% Sp, Cb, Argentopentlandite, Fletcherite	X	
	LG87	0.77	0.01	10		90			
Guyer 630-700°C	LG 69	0.34	0.03	99		1		X	X
	LG 70	1.70	0.01	60		40	Sp, Bi-Te Phase	X	X
	LG 71		0.01		50	50			
	LG 73	1.86	0.03	96		4			
	LG 75	0.60	0.01	95		5			
	LG 76	0.43	0.08	98		2			
	LG 78	0.79	0.01	95		5			
	LG 80	0.32	0.09	98		2		X	X
	LG 81	0.19	0.01						
	LG 84	2.26	0.02	83		12	5% Mll, Pn, Cv, Violarite	X	X
	LG 85	0.56	0.08	99		1			
La Forge 700-750 ± 40°C	LG 51		0.01						
	LG 52	0.35	0.01	100				X	
	LG 54	0.13	0.01						
	LG 55		0.01						
	LG 56	0.63	0.01	90		10	Mol	X	
	LG 57	1.22	0.04	85		15			
	LG 59	0.23	0.04	98		2	Mol, Galena	X	X
	LG 60	1.15	0.03	98	1	1		X	X

Table 1 Sulfide characterisation and quantification of the metabasalt thin sections. Details of Au and S whole rock composition and analytical methods are attached. S detection limit is 0.01 %wt.

From this relative quantification elaborated at the reflexion and electron microscopes, the total mass of each sulfide has been calculated using whole rock S concentrations (Figure 5). Each sulfide phase percentage represents a percentage of the measured S mass plus an Py-equivalent stoichiometric value of iron. The sulfide phase percentage are therefore an estimation based on the whole rock geochemistry and the petrographic observations. The diagrams exhibit Py concentrations are variable in lower temperatures, that are converging to a roughly constant median value when temperature increases. Po and Ccp are more abundant in the lower metamorphic group. Po progressively disappear from the samples in higher temperatures.

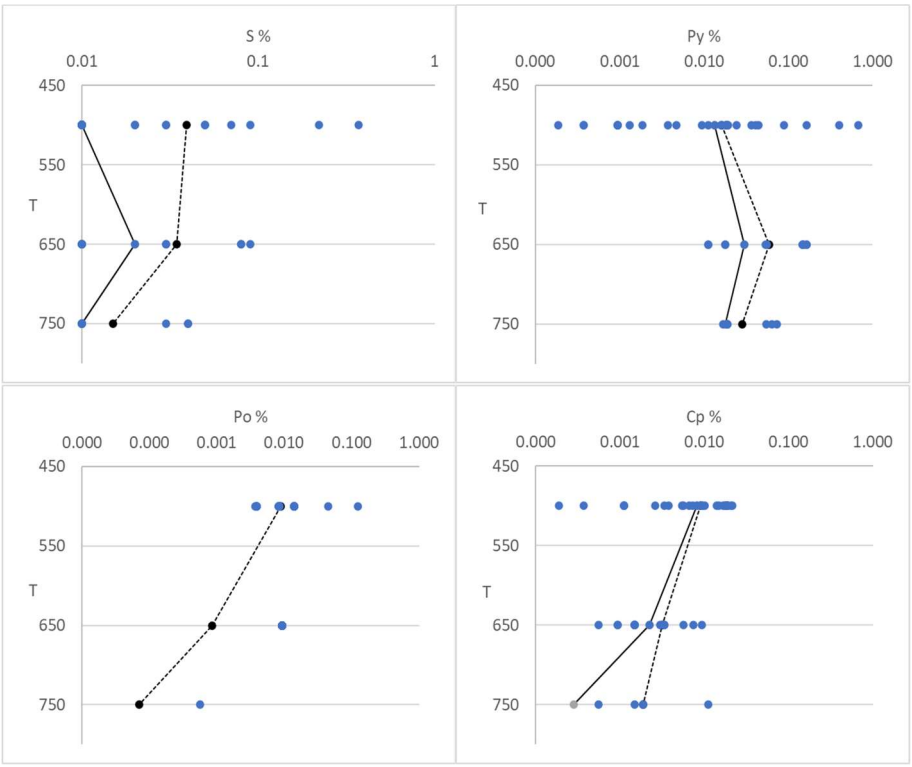


Figure 5. Sulfide content of the samples by metamorphic temperature, from visual estimation about measured S content. The solid curve connects the median values of each group, and the dashed curve connects the average values.

The petrographic study conducted in the reflexion and electron microscope is summarised below, providing details of the sulfide populations, associations and textures.

Yasinsky

The Yasinsky basalts with the lower metamorphic grade in the collection, at metamorphic temperatures of 480-530 ± 40°C, present average Py:Po:Ccp relative proportion of 52:9:39 in the 29 studied thin sections. Pyrite is present in 25 of the 28 sulfide-bearing samples, and it is the major sulfide in 16 of them, which are also the samples with the highest S %wt values, with the exception of LG02 and LG23, the only samples of the whole set dominated by pyrrhotite. 10 of the 23 samples with whole rock sulfide content at detection limits have chalcopyrite as the most abundant sulfide, which is also present in all the other samples, with one exception. Pyrrhotite is present in 7 of the 29 samples and the major phase in the above-mentioned two sections. Traces of millerite and sphalerite have been observed in two different samples.

In these samples, Pyrite textures are highly variable. Grain size varies from a few tens of microns to 0.5 mm and is generally subhedral, with euhedral crystals and anhedral oikocrysts with abundant silicate inclusions. It is frequent to find fine-grained aggregates with abundant inclusions surrounded

by euhedral crystals (Figure 6 D), which gives a rough or dirty-looking appearance to the grains. Some samples record a more intense development of the pyrite blasts, with more common euhedral shapes. Pyrite is always associated with chalcopyrite smaller grains or inclusions, occasionally associated with magnetite rims and occasionally with millerite. Chalcopyrite appears as rounded inclusions in pyrite grains, as euhedral very fine grains in the matrix, or is associated with other sulfide phases such as pyrrhotite. It also appears as the most abundant sulfide phase in LG86, where it is associated with sphalerite rims and many accessories in the disseminated sulfide-rich proximity of the coarse grains, such as argentopentlandite, cobaltite or fletcherite. Pyrrhotite appears as subhedral grains with frequent fractures and mild oxidation along its cleavage and exhibits occasional pentlandite exolutions. It appears in a few occasions associated with pyrite in replacement relations (Figure 7C and D), where the direction of the replacement is not always easy to determine. In some occasions, the pyrrhotite grains resulting from the replacement of the pyrite have different crystal shapes, sometimes preserving pyrite fracture style and then showing a clearer pyrrhotitic cleavage, which points to a complex pyrite-pyrrhotite replacement history previous to the latest stage (Figure 7A and B). The sulfides in the set are subject to different degrees of oxidation.

Guyer

Pyrite is the major sulfide phase in the amphibolitic group with metamorphic temperatures of 630 to 700 °C, and the most abundant one in 9 of the 11 thin sections, being the two remaining almost depleted in sulfide. The relative Py:Po:Ccp are in this group 82:5:13. Chalcopyrite is the second ubiquitous sulfide, associated with pyrite and in similar textures to the previous metamorphic groups. Pyrrhotite appears only rarely as for example, a rounded inclusion within an amphibole grain, probably representing the paragenesis before the interaction between sulfide and metamorphic fluids. Once again, sulfides are subject to different degrees of oxidation.

Pyrite shows a wide range of textures (Figure 8), from inclusion-rich idiomorphic to allotriomorphic grains and aggregates to close myrmekitic associations with chalcopyrite. It also appears with micro aggregate textures, probably as a result of late retrograde replacement (Figure 8 H). Chalcopyrite appears associated with other sulfides or as finer disseminated individual grains and generally shows differential resistance to oxidation against other sulfide phases (Figure 8 A). It also appears associated with 1 µm Au-bearing high electronic density Bi-Te exsolutions in the thin section LG 70, which have been identified on three occasions (Figure 8 E and F). It is worth mentioning the Ni-rich sample LG 84, with a significant amount of millerite and tich in Sulfide textures (Figure 8 D, G and H).

La Forge

The La Forge set of samples appears significantly depleted in sulfides, with 5 out of the 8 samples at sulphur detection limits, of which 3 thin sections have no visible sulfide grains in them. Pyrite is the major phase in all the sulfide-bearing samples, followed by chalcopyrite. Pyrrhotite appears as a trace in one sample on a single occasion. The relative abundance of Py:Po:Ccp is then 94:0:6.

Pyrite shows frequent rounded subhedral shapes (Figure 9 D, E and F), and abundant silicate and chalcopyrite inclusions. It also appears as clean crystals with fractures along orthogonal cleavage (Figure 9 B) or as fine-grained aggregates (Figure 9 A). Occasional rounded pyrite grain edges are rimmed by barite and iron oxides. Chalcopyrite is frequently included in pyrite grains or associated with them. The only pyrrhotite occurrence is a 20 µm concave-sided inclusion in pyrite, which constitutes evidence for the retrogradation of high metamorphic grade pyrrhotite into pyrite.

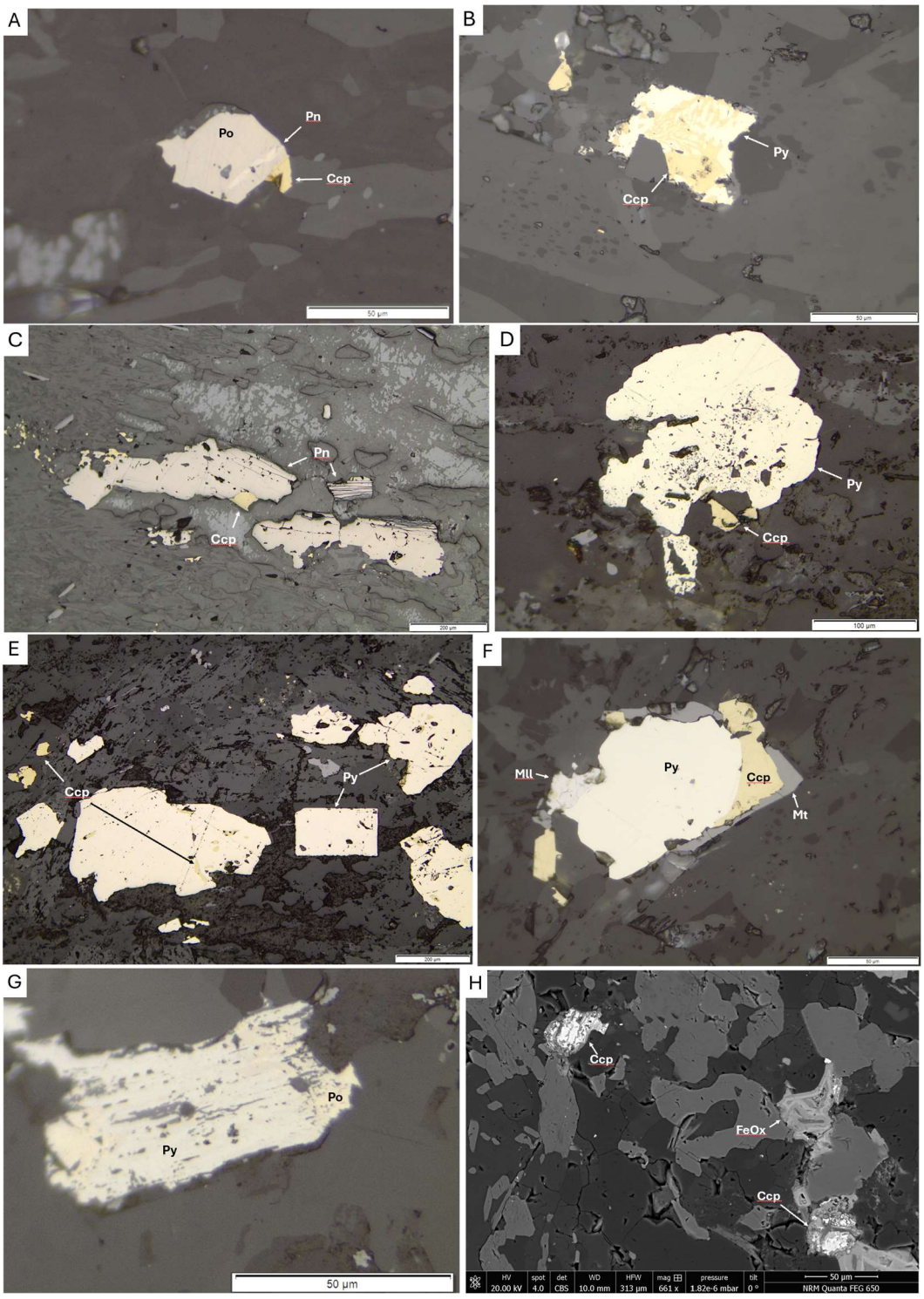


Figure 6. Yasinsky group. A) Very fine grain in the rock matrix of Po, Pn lamellae and Ccp assemblage, LG23. B) Py-Ccp myrmekitic intergrowth from LG 21. C) Coarse Po-Ccp associated with folded veins, LG23. D) Fine-grained Py core aggregate with large euhedral grains at the rim from LG27. E) Euhedral to subhedral grains of Py, with abundant Ccp inclusionLG27, F) Py-Ccp-Mi-Mt association LG21. G) Py-Po association with Py core and Po rims. Py exhibits relict planar cleavage from LG 32. H) Advanced oxidation of sulfides, with only Ccp resisting the weathering-alteration, from LG 33

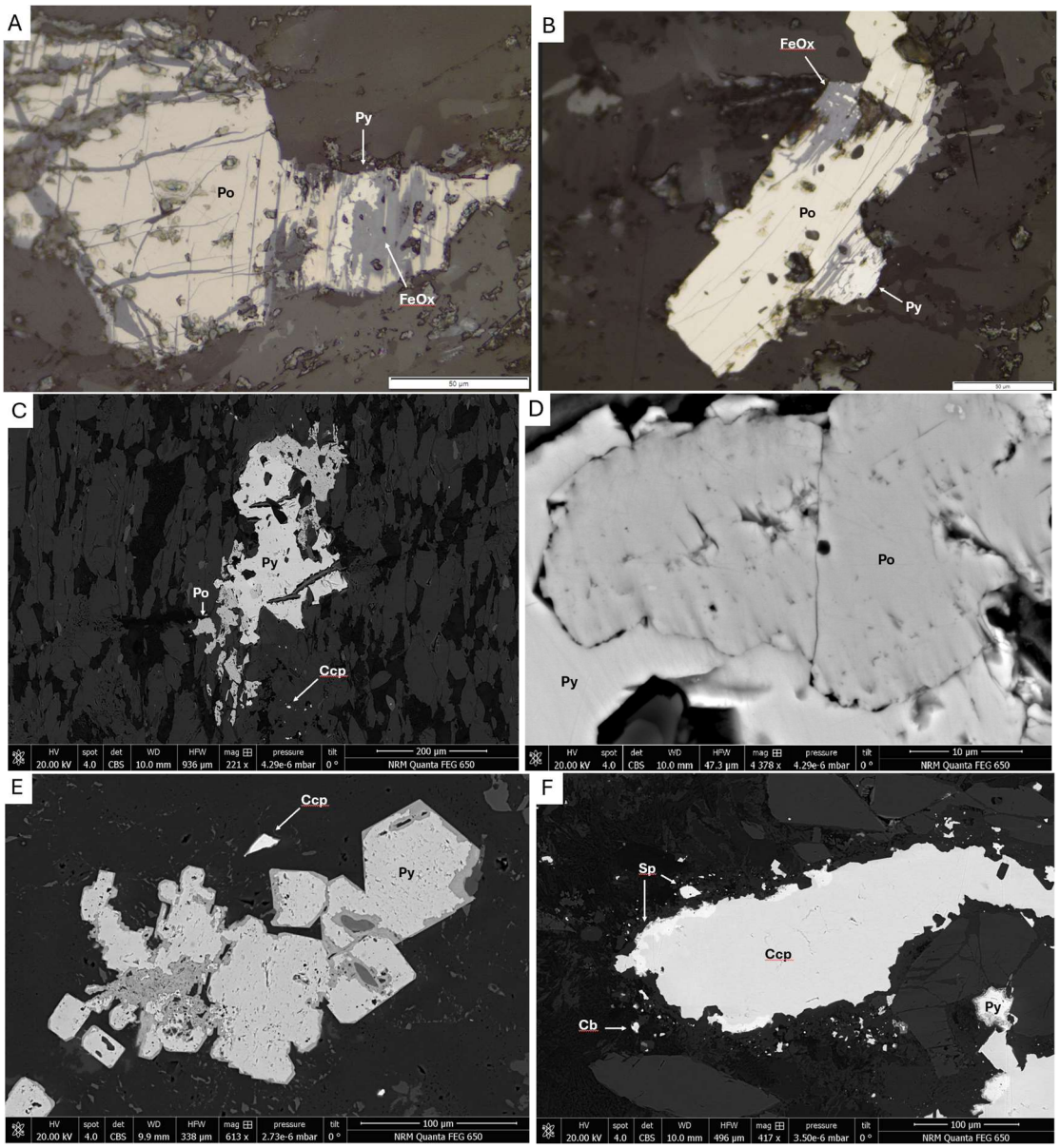


Figure 7. Yasinsky Group. A) Po replacing Py, preserving the cubic fractures of the precursor grain, possibly a Py metamorphic blast, and a Py inclusion indicating the reaction was not completed. B) Partially fractured and oxidised Po replacing Py, where the crystal grains exhibit pyrrhotitic shapes, from LG 02. C) Anhedral Py-Po replacement association and D) detail of the replacement front from LG 04. F) Moderate oxidised subhedral-euhedral Py aggregates with abundant silicate and minor Ccp inclusions from LG 10. H) Coarse grain of Ccp from the Ccp-rich LG 86. Sphalerite rims around Ccp and races of cobaltite, pyrite and fletcherite in the main sulfide grain surroundings.

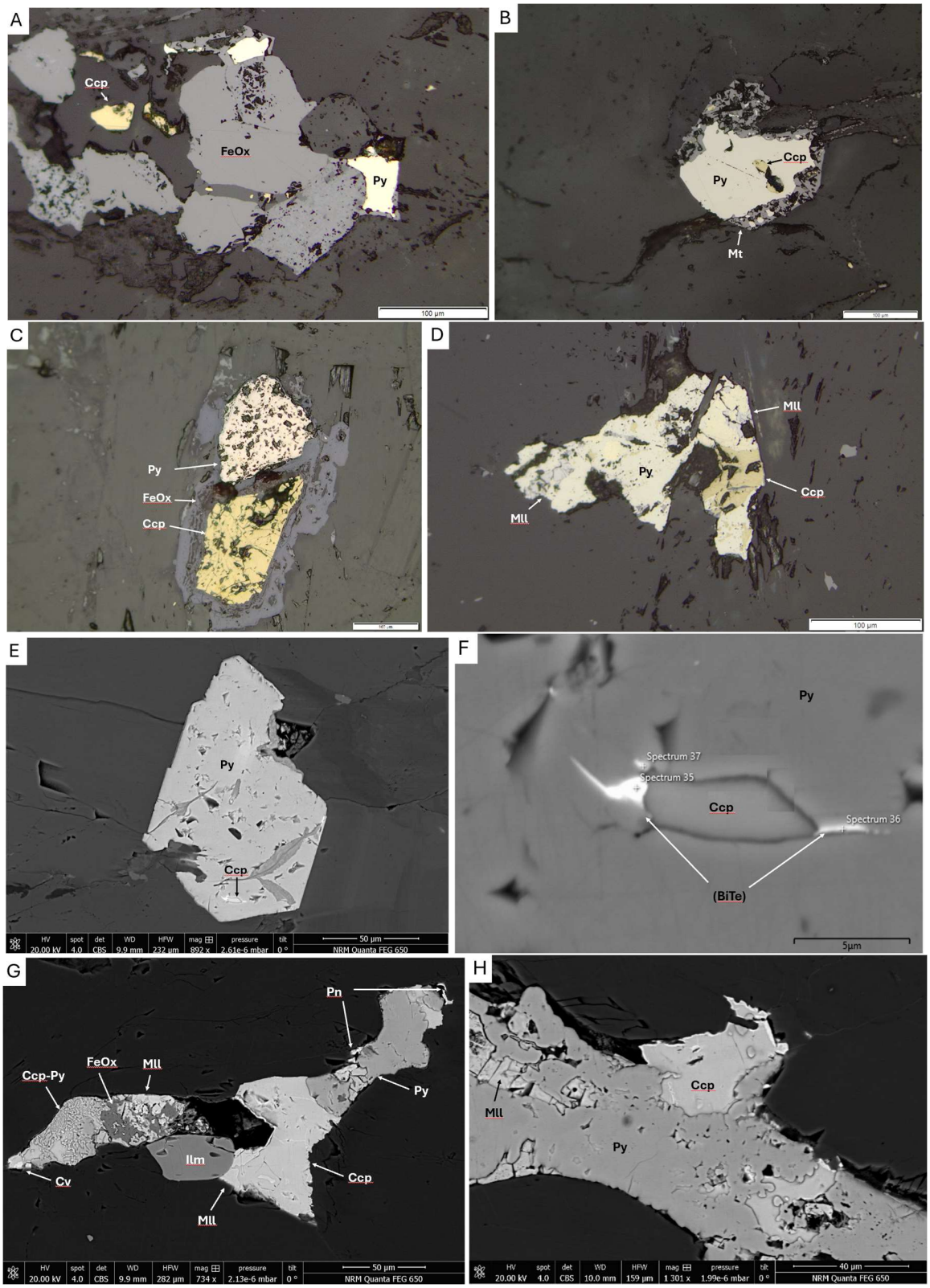


Figure 8. Guyer. A) Oxidation of Py aggregates with relict grain boundaries and inclusion-rich nucleus from LG80. B) Py-Ccp-FeOx-Mll association and C) Py-Ccp association from LG 70. D) Py-Ccp-Mll association from the Ni-rich sample LG 84. E) Py grain rich in silicate and Ccp inclusions, including Au-bearing Bi-Te segregation associated with Ccp inclusion, detail in F), from LG70. G) and H) Textural details of the sample LG 84: Py-Ccp intergrowth textures, Ccp-Mill association, or microgranular Py texture, possibly resulting from retrograde Po replacement.

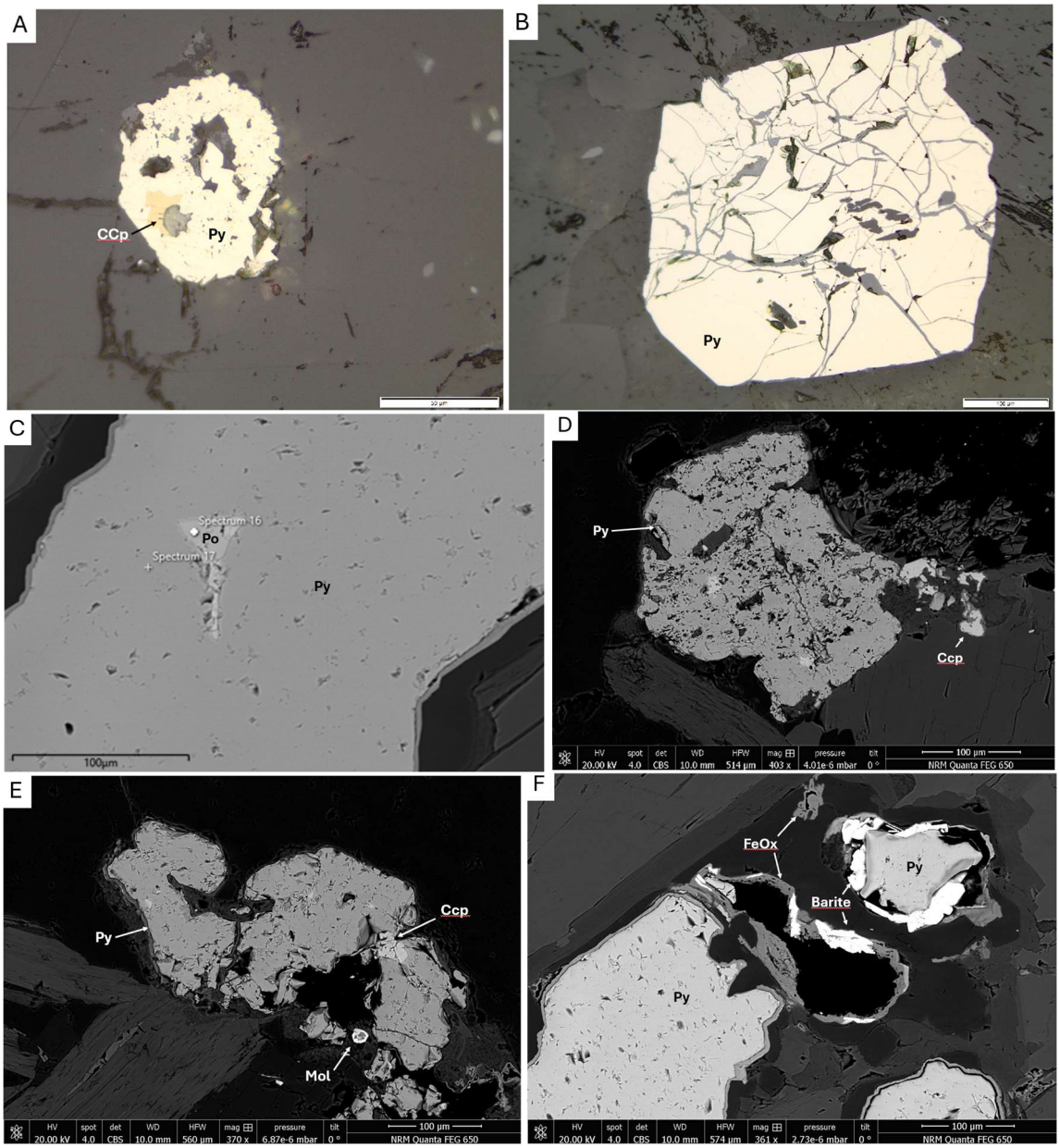


Figure 9. La Forge. A) Py aggregate with Ccp inclusions, possible retrograde replacement texture of Po, and B) fractures along orthogonal cleavage in a metamorphic Py blast, both from LG 59. C) Po inclusion in Py grain, from LG 60. D) and E) show anhedral-subhedral Py aggregates rich in silicate and Ccp inclusions from LG 56. F) Barite and iron oxide rims around rounded Py grain edges from LG 60.

The relative sulfide abundance variation along metamorphic grade is represented in Figure 10. Note those proportions do not represent the average proportion of the sulfide population, as they are not referred to the total sulfide abundance of each sample.

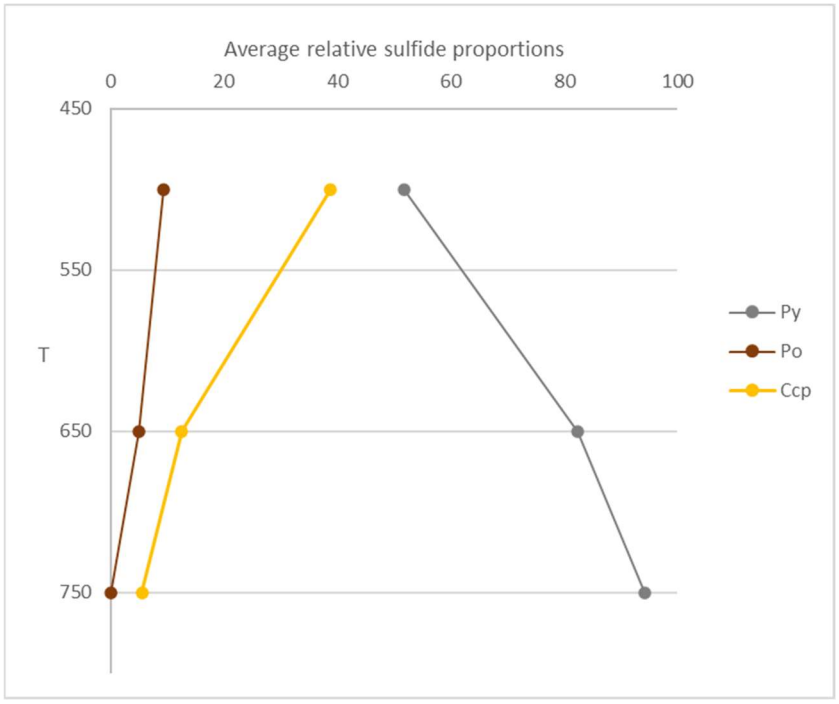


Figure 10. Average Py:Po:Ccp variation through metamorphic grade.

5.2. In situ Determination of Gold and Trace Element Concentrations in Sulfides

At the analytical stage, 207 punctual analyses were obtained by laser ablation of the main sulfide phases identified in the petrographic study, of which 134 were conducted over pyrite grains, 44 on chalcopyrite, and 29 over pyrrhotite. The average, median, minimum and maximum values for each phase in each metamorphic group are summarised in the Table 2 and visualised in Figure 11.

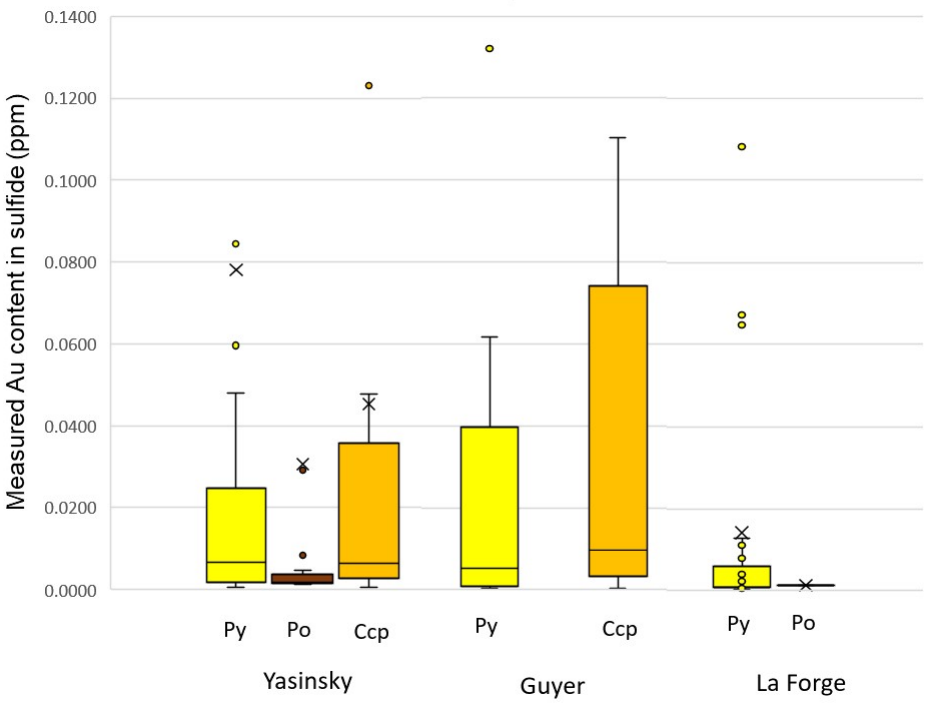


Figure 11. Box and whisker plot of the analysed gold content of the main sulfide phases by metamorphic group.

The analysis indicates that in the Yasinsky formation, at the low metamorphic temperature group, the measured pyrite grains host on average 2.4 times higher concentration of gold than pyrrhotite grains and 1.71 times higher than chalcopyrite. In the Guyer formation, pyrite hosts 1.83 times the chalcopyrite gold concentrations, while no suitable Po grains have been found their ablation. At higher metamorphic temperatures, in La Forge formation, the pyrite contains 10.6 times more gold than the only analysed pyrrhotite remanent inclusion, but pyrite in La Forge contains 5.55 less gold that at the low metamorphic grade in Yasinsky.

The maximum gold value obtained during the data acquisition, attached at the end of the table was a 68ppm Au value (plus 4453 ppm Bi and 6722 ppm Te), recorded separately at the end of the table, obtained when shooting the Be-Te <1 µm exclusions in a 8 x 2 µm chalcopyrite inclusion in pyrite, with element ratios close to tellutobismuthite end of the solid solution (Figure 8 F). As the spot size of the ablation was, in that case, 12 µm, the measurement can only qualitatively indicate the association of gold with the Te-Bi phase. However, if we assume all the Au would be hosted by the micron-sized Bi-Te phase; its Au concentration would be 0.6% or 6000ppm Au.

Pyrite	**(ppm)**	**Au**	**Ag**	**As**	**Co**	**Ni**	**Cu**	**Zn**	**Se**	**Pd**	**Sb**	**Te**	**Bi**
Yasinsky (n=59)	Average	0.0780	30.99	45.84	2997.73	6217.22	994.82	88.56	130.55	0.98	6.21	7.76	1.08
	Median	0.0066	0.48	19.05	773.82	542.48	58.95	1.33	102.80	0.93	0.41	1.49	0.34
	SD	0.4240	79.67	66.03	4599.28	13866.68	2703.82	317.31	94.80	0.40	12.05	15.25	1.64
	Max	3.0100	334.82	251.83	20340.12	55069.21	18006.61	1896.90	335.52	2.31	46.28	71.73	6.61
	Min	0.0005	0.02	0.48	27.67	58.68	0.23	0.39	12.94	0.47	0.00	0.00	0.01
Guyer (n=48)	Average	0.1794	11.39	407.77	4217.63	5751.15	2894.00	58.54	134.88	0.92	10.86	24.68	5.29
	Median	0.0053	0.20	4.99	454.74	678.20	18.31	0.59	116.94	0.68	0.16	4.30	1.82
	SD	0.7449	37.50	1586.39	10840.87	24647.37	8381.16	335.82	145.29	0.86	25.75	39.27	7.53
	Max	5.1200	252.71	10768.37	70058.38	172802.42	49192.84	2355.86	824.84	5.17	121.53	127.18	30.92
	Min	0.0004	0.01	0.27	0.22	3.54	0.16	0.32	4.46	0.49	0.03	0.34	0.01
La Forge (n=37)	Average	0.0141	4.08	6.30	1902.18	1671.67	870.96	10.77	73.27	0.73	0.11	10.44	1.97
	Median	0.0008	0.03	2.59	1502.81	1320.53	3.01	0.50	41.40	0.70	0.08	0.71	0.01
	SD	0.0322	11.02	9.14	1760.14	1882.34	2716.04	55.78	57.70	0.12	0.16	25.78	4.44
	Max	0.1426	53.74	46.75	5191.16	10495.64	12359.10	344.99	212.83	0.97	1.03	122.69	16.07
	Min	0.0003	0.02	0.37	0.08	0.90	0.23	0.23	11.62	0.54	0.03	0.46	0.00
Pyrrhotite	**(ppm)**	**Au**	**Ag**	**As**	**Co**	**Ni**	**Cu**	**Zn**	**Se**	**Pd**	**Sb**	**Te**	**Bi**
Yasinsky (n=38)	Average	0.0306	9.22	8.01	4251.69	18712.25	584.34	30.30	167.54	2.53	3.13	4.55	1.1492
	Median	0.0019	0.39	1.36	943.65	8469.96	7.48	1.59	154.17	1.91	0.26	1.52	0.0740
	SD	0.0977	28.86	22.90	14127.00	38209.33	1085.06	69.77	54.21	1.37	10.21	8.74	3.2070
	Max	0.3890	153.78	118.02	76198.80	209440.06	4342.14	314.61	344.24	6.37	42.99	32.23	15.1400
	Min	0.0012	0.05	0.84	323.96	4778.79	0.51	0.98	114.00	1.05	0.08	0.98	0.0166
Guyer (n=0)		-	-	-	-	-	-	-	-	-	-	-	-
La Forge (n=1)	Value	0.0013	23.99	1.91	144.27	1460.05	2153.71	3.69	162.22	1.17	0.18	2.70	0.05
Chalcopyrite	**(ppm)**	**Au**	**Ag**	**As**	**Co**	**Ni**	**Cu**	**Zn**	**Se**	**Pd**	**Sb**	**Te**	**Bi**
Yasinsky (n=27)	Average	0.0456	33.21	6.71	198.87	553.90	192099.24	277.89	120.93	3.94	0.79	3.67	0.67
	Median	0.0060	15.88	1.98	53.89	136.05	262818.44	78.35	125.85	2.84	0.45	3.08	0.15
	SD	0.1495	39.87	15.83	283.26	1012.07	120764.67	509.19	82.00	4.43	1.00	2.50	1.24
	Max	0.7970	159.29	74.35	1185.14	4281.94	323052.59	2472.12	328.11	21.00	5.32	12.27	5.95
	Min	0.0006	0.02	0.37	0.31	1.75	0.27	0.54	19.10	0.40	0.08	0.83	0.02
Guyer (n=17)	Average	0.0816	50.31	74.48	2152.53	1620.72	233994.28	292.28	142.59	3.20	12.46	14.55	264.75
	Median	0.0097	26.32	2.35	0.65	8.61	291954.80	217.24	122.88	3.58	0.71	3.47	0.42
	SD	0.1691	52.81	187.68	5500.11	4317.76	135918.35	408.43	92.34	1.79	29.88	24.37	1047.32
	Max	0.5340	158.34	593.40	21914.11	15964.89	418075.38	1785.14	359.86	8.03	94.04	84.23	4453.98
	Min	0.0004	0.38	0.27	0.30	2.00	547.22	4.96	6.91	0.40	0.02	0.46	0.04
La Forge (n=0)		-	-	-	-	-	-	-	-	-	-	-	-
LG 70, Py-Ccp-Bi-Te inclusion		68.20	65.11	962.63	1088.16	3120.11	15832.74	10.72	411.09	0.53	0.78	6722.75	4453.98

Table 2 Trace element content in main sulfides by the formation and metamorphic temperature group.

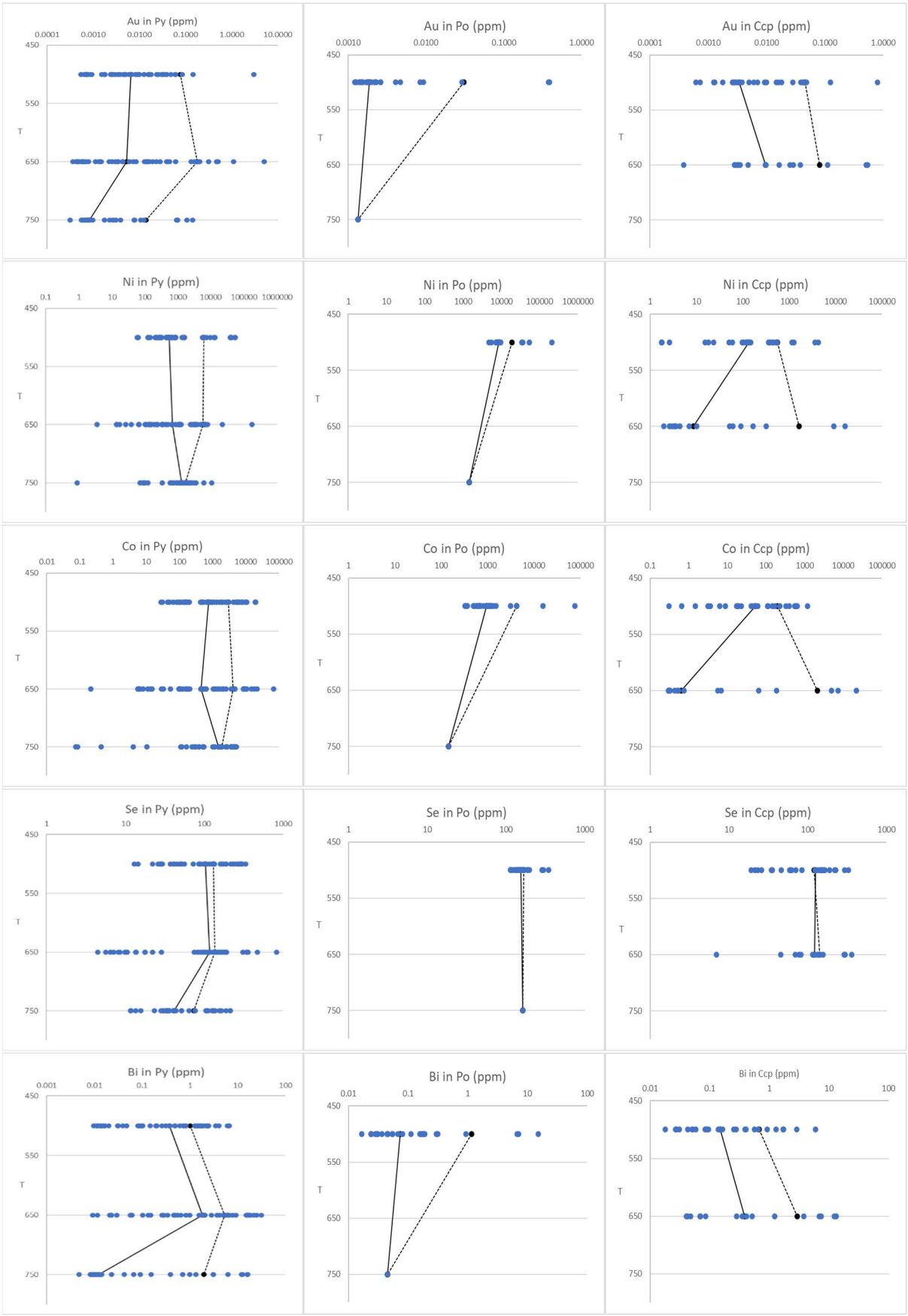


Figure 12. Trace element concentrations in different sulfide minerals pyrite (Py), pyrrhotite (Po) and chalcopyrite(Ccp) plotted against metamorphic temperature of the host sample. The solid curve connects the median values, and the dashed curve connects the average values.

The data indicates the median content of gold in pyrite stays continuous between upper greenschist to amphibolite facies, in Yasinsky and Guyer formation, and drops in the upper amphibolitic samples of La Forge, showing a moderate depletion with increasing metamorphic grade. On the other hand, chalcopyrite Au content is slightly higher in Guyer than in Yasinsky. Se content in pyrite shows a similar distribution as gold, with decreasing concentrations at high metamorphic temperatures, while staying constant in chalcopyrite. Bi shows very variable concentrations in sulfides without clear signs of depletion along prograde metamorphism (Figure 12).

The larger grain size and abundance of the pyrite population made possible the selective in situ measurement of 35 grain cores and 36 grain edges. The median gold content of the pyrite cores is higher than the median rim values at greenschist-amphibolite facies and seems to homogenise in upper amphibolitic facies (Figure 13)

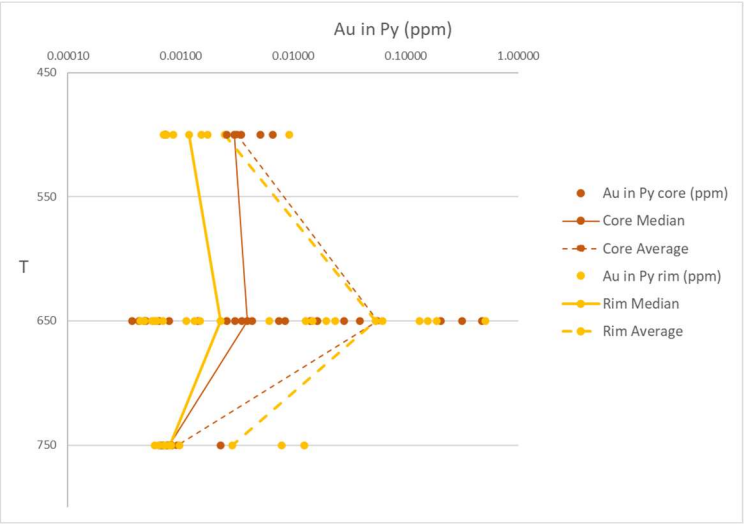


Figure 13. Au content in pyrite grain cores and rims. The solid curve connects the median values of each group, and the dashed curve connects the average values.

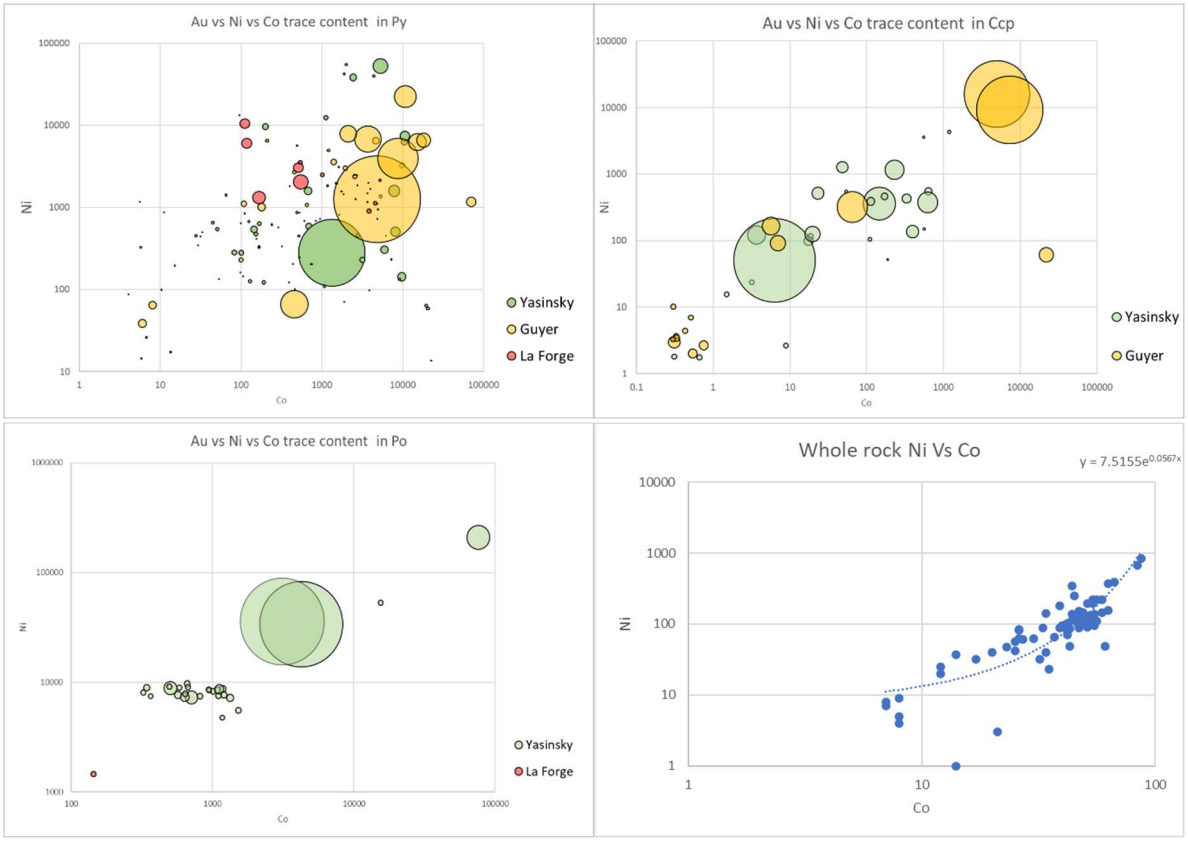


Figure 14. Ni vs Co vs Au by sulfide phase and metamorphic texture. Bubble diameter represents Au concentrations. The last diagram represents the whole rock Ni vs Co trend of of the samples set.

The Ni and Co trace content ratios of and chalcopyrite tend to align with the whole rock ratios even along the different metamorphic temperatures, while Ni and Co ratios in pyrite seem more dispersed (Figure 14). Ni and Co trace content is more heterogeneous in pyrite and chalcopyrite in each metamorphic group, and there is no clear Ni or Co depletion in the different sulfides with the increasing metamorphic temperatures.

6. DISCUSSION

6.1. Mineralogical Framework and Textural Interpretation

The aim of this investigation was to explore whether the mineralogical framework we use to explain mobilisation of gold during prograde metamorphism in metasedimentary rocks is applicable in metabasaltic rock sequences. In the metasedimentary scenario, with the critical study on the Dalarian sequences in Scotland, Pitcairn et al., 2015 showed a clear prograde transformation of the primary Py into Po, not affected by retrograde reactions, where the relative abundance of sulfides clearly aligns with the suspected process of depletion. Similar results have been observed in metasedimentary rocks in the Archean Abitibi terrane in Canada (Leventis, 2017; Pitcairn et al. 2021). The petrographic study of the metabasalts presented in this study suggests some similarities and overlap between the mineralogical systems observed in metasedimentary and metabasaltic rocks, but that there are also significant differences in the abundances of different sulfides and their behaviour during metamorphism. At least four stages of sulfide formation and transformation and two of sulfide breakdown have been identified in the studied metabasalts. These observations require a new framework for the metavolcanic rocks, developed from a combination of the findings of Patten et al., 2016, and the observations of this project.

Prior to metamorphism the sulfide evolution start with the primary magmatic sulfide crystallisation, where the cooling of the sulfide droplets would produce the Isomorphic Solid Solution + Monosulfide Solid Solution association (ISS+MSS), stable at high temperatures later reaching equilibrium with the Po-Pn-Ccp assemblage (Figure 15; Patten et al. 2016). Experimental studies show that Au tends to concentrate preferentially in the residual ISS melt in the primary sulfide formation scenario, subsequently forming chalcopyrite (Patten et al., 2013). At this stage the gold should reside in a combination of chalcopyrite and pyrrhotite. During synvolcanic metasomatism interaction between the sulfide and syngenetic fluids produces a pyrite and chalcopyrite dominated assemblage and at this stage the Au is preferentially in pyrite (Patten et al., 2016).

It is not clear whether this metasomatism is a pervasive process along metabasaltic terrains, or if it is rather restricted to structural domains with the convenient fluid availability. This point is key to address the question of many and which sulfide assemblages are entering the metamorphic cycle. Tomkins, 2016, indicates that the window for the Py-Po transition is quite restricted to the transition of greenschist to amphibolitic facies at lower pressure, as the process is controlled not only by temperature and pressure, but by the availability of H_2O, sourced in those conditions by the breakdown of chlorite. Other studies on metabasaltic terrains (Pitcairn et al., 2015) pyrite seems to be the dominant sulphide in greenschist facies. However, is rather difficult to discern and generalise if the pyrrhotite in observed in the Yasinsky group is primary or if it is already a metamorphic product that survived the retrometamorphism, as the metamorphic grade of the Yasinski group rocks is close to the chlorite breakdown window, or if the pyrite in the same low grade samples is a syngenetic metasomatic product or a result of retrograde metamorphism. These different alternatives, which all seem to be possibly happening at the same time in this terrain and represented in the sample set, set up a range of different initial conditions of the processes to study, or in other words, different inputs to the metamorphic cycle.

This study's low metamorphic grade samples show that pyrrhotite contain 1.4 times lower gold concentrations than the chalcopyrite, and at the same time, pyrite contains 1.7 times more gold than

the chalcopyrite. This distribution indicates that the early trace element distribution in the magmatic environment has been substantially transfigured during metamorphism in the bulk of samples.

During prograde metamorphism it is expected that periods of pyrite growth and annealing eventually lead to replacement by pyrrhotite (Craig & Vokes, 1993). The Py-Po transition, which requires an interaction with a fluid phase, can occur in a wide range of temperatures, from early greenschist to upper amphibolite facies, depending on several variables. After reaching the metamorphic peak, retrograde recrystalisation can occur where Po can be entirely replaced by Py again. These sulfide transformation processes can be interrupted by leaching episodes, starting at the syngenetic hydrothermal circulation. Figure 15 offers the textural keys to interpret this process. Similarly, sulfide oxidation episodes can also subtract S and Au from the system. Chalcopyrite, however, seems to constitute a refractory repository of gold, with higher differential resistance to early hydrothermal alteration, prograde and retrograde transformations, and eventual leaching and oxidation. The samples with the five highest Au/S ratios (LG 31, 37, 38, 39 and 41), belonging to the group Yasinsky, are dominated by traces of Ccp. The textural interpretation of the key samples is shown in Table 3 including the interpretation of primary, prograde and retrograde assemblages. The mineral paragenesis in most of the samples, specially in the high metamorphic grade ones, indicates an intensive retrograde recrystalisation of the sulfides. It is assumed that Po was formed in the prograde stage and therefore the abundance of Py indicates intensive retrogression. This is supported by the textural evidence where Py contains inclusions of Po (Fig. 9; Table 3). Pyrrhotite is much more abundant in the lower metamorphic grade samples than in those of higher grade and is essentially absent in the higher metamorphic grade samples. The intensity of the retrograde recrystalisation masks the prograde evolution of the sulfides, making impossible to quantify relative proportions of sulfides during the prograde metamorphic stage.

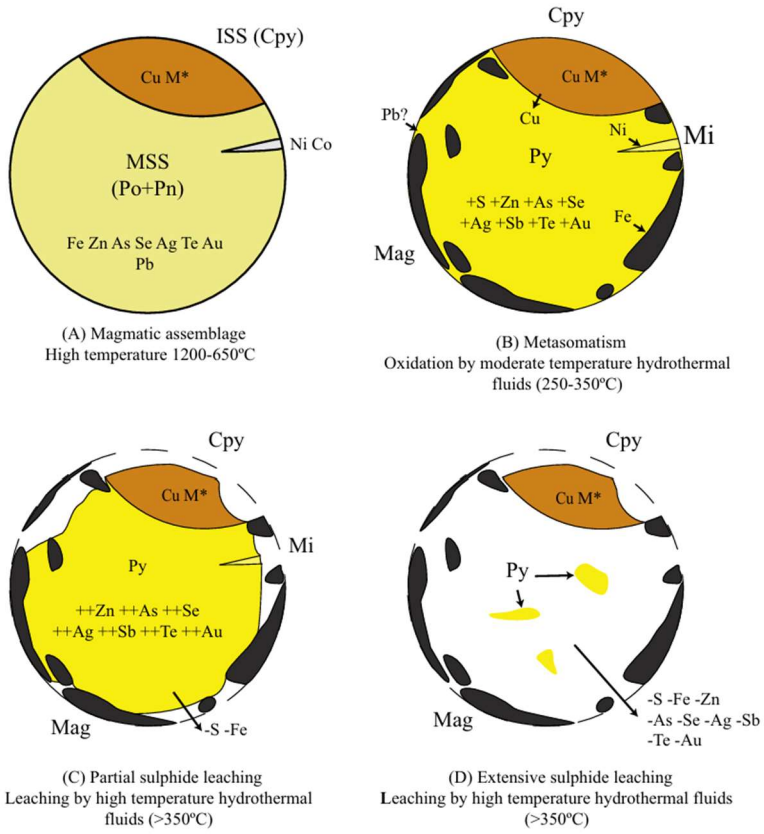


Figure 15 Different paragenesis and metal distributions entering the metamorphic processes, formed by metasomatism and leaching of primary magmatic assemblages in basalts during syngenetic hydrothermal alteration. Starting from (A) ISS-MSS,

exsolving subsolidus into (Po-Pn) and Ccp. Interaction with hydrothermal fluids at different temperatures will produce (B) sulfide metasomatization and metal diffusion, as well as progressive leaching in (C) and (D) as temperatures and intensity of the process increase. From Patten et al. 2016.

		Analytical methods	Relative sulfide abundances	Texture	Interpretation	Primary Textures	Early hydrothermal Replacement	Prograde Py formation	Prograde Po formation	Retrograde Py replacement	Advanced weathering or leaching
Yasninsky	LG 02	SEM-EDS, LA-ICP-MS	48% Po, 29% Py, 23% Ccp	Abundant clean Po with oxides along foliation. Remanent inclusions of Py in Po grains.	Metamorphic Po is replacing Syngenetic Py.				x		
	LG 04	SEM-EDS	73% Py, 25% Po, 2% Ccp	High variation of Py textures: Py-Po replacement textures, patchy anhedral grains with abundant silicate inclusions, and subhedral grains with Ccp inclusions.	It is not clear if Po is replacing Py (prograde reaction) or if Py is replacing Po (retrograde reaction). Textural evidence of Py metamorphic growth.			x	?	?	
	LG 10	SEM-EDS, LA-ICP-MS	85%Py, 15% Ccp, traces of Cv and Cb	Coarse euhedral Py grains with Ccp inclusions and oxide rims. Euhedral Grains of Py around finer aggregates.	Evidence of prograde Py formation and complete retrograde replacement of any prograde Po, if it was formed.			x	?	x	
	LG 21	SEM-EDS, LA-ICP-MS	98% Py, 2% Ccp, traces of Mi, Bornite	Rounded Py with few Ccy inclusions, plus euhedral Ccp in the matrix. Py-Ccp myrmekitic textures. Grains showing Py-Ccp-Mi-Mt association	Evidence of primary textures: Py-Ccp intergrowth textures, where early metasomatic Py is replacing Po, and grains with Py-Ccp-Mi-Mt association, resulting from Po-Pn-Ccp primary association.	x	x				
	LG 23	SEM-EDS, LA-ICP-MS	94% Po, 5% Ccp, 1% Py, traces of Pn	Unusual coarse Po-rich sample. Coarse subhedral Po associated with folded veins and fine-grained Po in the matrix. Pn lamellae and inclusions in fine Po grains. Traces of Py replacing Po grains from exfoliated edges, plus fine-grained Ccp.	Possible primary Po preserved. Fine grains of Po with Pn lamellae associated with Ccp. Larger Po-Pn-Ccp in folded veins. Evidence of later Py replacing Po, possibly retrograde	x				x	
	LG 27	SEM-EDS, LA-ICP-MS	97% Py, 3%Ccp, traces of Sp and Galena	Coarse eu-subhedral Py and finer Ccp. No Mt associated with Py.	Retrograde Py is completely replacing the primary and/or metamorphic Po.			x		x	
	LG 32	SEM-EDS, LA-ICP-MS	51% Py, 27% Ccp, 22%Po, traces of Mill and Sp	Heterogeneous Py textures. Subhedral py with Ccp inclusions, Patchy anhedral Py grains with abundant silicate inclusions, and relict cleavage in Py grains partially or totally replacing Po. Few cleavage plains in Po grains preserved. Finer-grained Ccp and traces of Mi.	Py partially replacing primary and/or metamorphic Po. Ni-rich Py grains, preserving relict cleavage of Po, are additional evidence of the replacement. Patchy grains of Py with silicate inclusions are evidence of the metamorphic growth of Py.			x			
	LG 33	SEM-EDS	100% Ccp	Few traces of Ccp, advanced oxidation	High gold and low sulphur samples. Ccp is only a refractory phase resisting sulfide consumption processes as a gold repository.						x
	LG 39	SEM-EDS	100% Ccp, traces of Mol	Few traces of Ccp and Mo, advanced oxidation							x
	LG 86	SEM-EDS	94% Ccp, 5% Sph, 1% Py, traces of Cb argentopentlandite and fletcherite	Coarse Ccp with Sph rims. Diverse trace speciation. Traces of anhedral Py.	Possible assemblage representing hydrothermal alteration under special conditions		?				?

		Analytical methods	Relative sulfide abundances	Texture	Interpretation	Primary Textures	Early hydrothermal Replacement	Prograde Py formation	Prograde Po formation	Retrograde Py replacement	Advanced weathering or leaching
Guyer	LG 69	SEM-EDS, LA-ICP-MS	99% Py, 1%Ccp	Fine-grained Py aggregates plus coarser euhedral Py grains surrounding them are associated with Ccp. Few myrmekitic inclusions of Ccp in Py.	Possible evidence of magmatic textures in Py grains, pointing them as early metasomatic replacement of Po. Evidence of Metamorphic Py formation around syngenetic Py.	?		x	?	?	
	LG 70	SEM-EDS, LA-ICP-MS	60% Py, 40%Ccp, traces of Sp and Bi-Te phase	Subhedral Py grains with oxide rims and Ccp and Ni-Co-Fe-S inclusions. Bi-Te-Au exsolutions around some Ccp inclusions. Some coarse Ccp grains	If formed, any primary or prograde Po is completely replaced by syngenetic or retrograde Py.			x	?	?	
	LG 80	SEM-EDS, LA-ICP-MS	98% Py, 2%Ccp	Partially oxidised Py with rounded Ccp inclusions	If formed, any primary or prograde Po is completely replaced by syngenetic or retrograde Py.			x	?	?	
	LG 84	SEM-EDS, LA-ICP-MS	80% Py, 15% Ccp, 5% Mi, traces of Pn, Cv	Complex Py-Ccp-Mi-Mt(±Ilm-Pn). Intergrowth of Py-Ccp	Py-Ccp-Mi-Mt assemblage representing early hydrothermal replacement of Po-Pn-Ccp. intergrowth myrmekitic Py-Ccp indicative of primary textures. Fine microcrystalline Py texture from late retrogradation of Po	x	x			?	
La Forge	LG 56	SEM-EDS	90% Py, 10%Ccp, traces of Mol	Subhedral to anhedral Py grains and aggregates with Ccp inclusions. Rims of oxides and barite	Similar texture to LG 60, so probable retrograde Py replacing metamorphic Po				x	x	
	LG 59	SEM-EDS, LA-ICP-MS	98% Py, 2%Ccp, traces of Mol and Galena	Subhedral to anhedral Py grains and aggregates with Ccp inclusions.	Textural indications of Py metamorphic formation and possible retrograde Py formation from Po.			x	?	?	
	LG 60	SEM-EDS, LA-ICP-MS	98% Py, 1% Ccp, traces of Po	Eu-subhedral Py grains with oxide-barite rims. Po inclusion in Py.	Evidence of retrograde Py replacing Po. Moderate late oxidation				x	x	

Table 3. Relative sulfide quantification, textural summary and textural interpretation of a representative sample selection used for SEM-EDS and LA-ICP-MS analysis.

6.2. Host minerals for Au

The in-situ gold content in sulfide measurements has been compared with the mineral quantifications and whole-rock compositions to identify the main hosts of gold in the samples. Results are shown in

Table 4. This approach for the inventory distribution among sulfide phases does not offer a satisfactory matching allocation of the gold inventory among the sulfide hosts. There are many reasons to explain this inadequacy. First, the sulfide quantification of a three-dimensional sample based on a bi-dimensional thin section is not based on a representative subsample. Secondly, gold is not homogeneously distributed at several scales, and the punctual analysis and number of them do not cover the variation ranges from a statistical point of view in all cases.

Group	Sample		Py	Po	Ccp	Total % of the Au inventory	Au in sample (ppb)
Yasinsky	LG02	%wt	0.009	0.052	0.027		0.231
		% inventory	160.2	41.5	135.1	**336.9**	
	LG10	%wt	0.015	0.0	0.009		2.781
		% inventory	13.8	0.0	30.2	**44.0**	
	LG21	%wt	0.009	0.0	0.006		0.467
		% inventory	15.6	0.0	22.3	**38.0**	
	LG32	%wt	0.022	0.029	0.039		0.671
		% inventory	134.7	1664.1	40.9	**1839.6**	
	LG23	%wt	0.000	0.175	0.010		0.294
		% inventory	0.0	166.1	15.0	**181.1**	
	LG27	%wt	0.076	0.0	0.077		2.419
		% inventory	14.4	0.0	9.9	**24.3**	
		Subtotal	56.5	312.0	42.2	**410.6**	1.144
Guyer	LG69	%wt	0.026	0.0	0.009		0.343
		% inventory	84.6	0.0	62.4	**147.0**	
	LG80	%wt	0.077	0.0	0.052		0.318
		% inventory	69.9	0.0	6.2	**76.0**	
	LG84	%wt	0.014	0.0	0.009		2.258
		% inventory	370.9	0.0	7.5	**378.3**	
	LG70	%wt	0.193	0.0	0.424		0.754
		% inventory	1461.8	0.0	367.6	**1829.5**	
		Subtotal	496.8	0.0	110.9	**607.7**	0.918
La Forge	LG59	%wt	0.026	0.0	0.0		1.147
		% inventory	18.8	0.0	0.0	**18.8**	
	LG60	%wt	0.009	0.003	0.0		1.699
		% inventory	1.3	0.2	0.0	**1.5**	
		Subtotal	10.1	0.1	7.2	**10.2**	1.423

Table 4. Approximation to gold inventory distribution among main sulfide phases, based on ultra-low detection limit whole rock analysis and in situ laser ablation gold measurements.

As the in-situ mineral analysis reveals, pyrite, the predominant sulfide in the samples, exhibits a progressive depletion of gold during prograde metamorphism. Although pyrrhotite appears to follow a similar trend, the statistical characteristics of the data do not permit to obtain a similar conclusion regarding its behaviour. The attempt to distribute the gold inventory among the sulfide phases indicates that, although these phases host a significant proportion of the gold content in the whole rock, there is potential for other unexamined gold allocations, such as native gold nanoparticles or high-grade/trace content phases like the Au-rich Te-Bi phase identified in this study. This gap in untested gold hosts appears to be particularly significant in the high-grade samples, where, on average, only approximately 10% of the total gold inventory has been accounted for within the sulfide phases.

In conclusion, we observe a progressive depletion of gold within the sulfide assemblages taken as a whole, which reflects the trend observed in the whole rock analysis. However, we are unable to identify or quantify the role of specific mineral reactions responsible for this gold loss, as the pervasive

retrogression obscures the state achieved during the metamorphic peak. Nonetheless, the prograde transformation of pyrite, which replaced primary pyrrhotite during the early syngenetic stages, into pyrrhotite remains as one of the main suspected mechanisms of gold deplection. The mobilisation of gold in scenarios where primary magmatic pyrrhotite was been preserved and subsequently subjected to the metamorphic cycle remains uncertain.

6.3 Significance of the findings

This study has successfully identified the successive sulfide paragenesis along the metamorphic path as one of the mechanisms contributing to the depletion of gold in metabasaltic rocks during prograde metamorphism. However, the retrogression affecting the sample set obscures a clear understanding of this process, preventing a definitive attribution of the Pyrite-Pyrrhotite transition as the primary controlling mechanism, although it remains a plausible explanation. The extent to which this retrograde modification of the sulfide assemblage has affected the whole-rock gold content is not clear. The depletion in Au from the whole rock samples follows what is observed in other terranes (e.g. Patten et al 2021) and the gold content in existing sulfide assemblage to some degree mimics the whole rock gold content. We expect therefore that the Au content of the sulfides has not changed hugely despite the retrograde recrystalisation.

Future research on this topic should begin with a careful selection of sampling locations, prioritizing metabasaltic terrains where samples are less affected by retrogression and where the metamorphic sulfide assemblages are better preserved. The inclusion of samples of lower metamorphic ranges would also inform more precisely of the primary paragenesis entering the metamorphic cycle. Once such a sample set is obtained, the focus should be on analysing sulfide phases with a higher statistical representation of each mineral phase throughout the metamorphic stages. This approach would provide a more statistically robust understanding of the gold inventory distribution, potentially indicating the necessity of extending investigations beyond sulfide phases to explore other possible gold hosts.

7. CONCLUSIONS

This study has provided significant insights into the role of sulfide paragenesis in the gold depletion observed in metabasaltic rocks within the La Grande Subprovince, Canada, during prograde metamorphism. By petrographic examination and in situ elemental trace content determination of a range of samples across different metamorphic grades, the research highlights the complexity of mineralogical transformations and their impact on gold mobilization. One of the central findings is the identification of changing sulfide paragenesis as a key mechanism that may contribute to the loss of gold during metamorphism.

The study finds that while sulfide phases, particularly pyrite and pyrrhotite, are important hosts for gold, the processes governing gold depletion are not completely clarified. The extensive retrogression observed in the samples, especially those subjected to higher metamorphic grades, complicates the interpretation of the mineralogical processes responsible for gold mobilization. Retrogression, characterized by the recrystallization of pyrite from pyrrhotite achieved at the metamorphic peak, appears to mask the evidence of the earlier prograde transformations that may have initially liberated

gold. On the other hand, Chalcopyrite appears as a refractory repository of gold, more resistant to the changing conditions along the metamorphic cycle.

This study also points that the pyrite-pyrrhotite transition, which has been well-documented in metasedimentary contexts, while plausible, cannot fully account for the observed gold depletion in the metabasaltic rocks of the La Grande Subprovince. The variability in sulfide textures and compositions across the different samples suggests that multiple processes, including syngenetic hydrothermal alteration, leaching, and late-stage retrograde metamorphism, have likely contributed to the redistribution of gold. This framework presents a complex view of the gold mobilization in metabasalts. The study also highlights the potential for other untested gold allocations, such as Bi-Te phases, to host gold. The behaviour in metamorphic conditions of those other phases has not been studied.

In conclusion, this thesis contributes with valuable information to the discussion on the topic in the literature, particularly about the understanding the behaviour of gold traces in metabasalts during metamorphism. While it advances the hypothesis that sulfide paragenesis changes are involved in gold depletion, it also highlights the complexity of these processes and the need for further research. Future studies should build on these findings by employing more refined locality and sampling selection that would allow a wider and stronger statistical analytical data acquisition, potentially expanding the scope to include other mineral phases that may act as gold hosts.

Acknowledgements

I would like to express my deepest gratitude to my supervisor, Dr. Iain Pitcairn, for his close support and guidance. Special thanks to Thomas Zack, from the University of Gothenburg and to Andreas Karlsson, from the Swedish Museum of Natural History, for their support during the analytical stage. I extend my heartfelt gratitude to those who endured my moments of struggle—my family, partner, and friends—with the hope that they will now partake in the quiet joy of this achievement.

8. REFERENCES

Craig J.R. and Vokes F.M, 1993. The metamorphism of pyrite and pyritic ores: an overview. Mineralogical Magazine, 57 (386): 3-18. doi:10.1180/minmag.1993.057.386.02.

Davis, D.W., Lafrance, I., Goutier, J., and Takam, F.T., 2014. Datations U-Pb effectuées dans les provinces du Supérieur et de Churchill en 2011-2012 – Ministère de l'Énergie et des Ressources naturelles. Report RP 2014-05, 61 p.

Fontaine, A., Dubé, B., Malo, M., McNicoll, V.J., Brisson, T., Doucet, D., and Goutier, J., 2015. Geology of the metamorphosed Roberto gold deposit (Éléonore Mine), James Bay region, Quebec: diversity of mineralization styles in a polyphase tectonometamorphic setting. Geological Survey of Canada, Open File 7852, p. 209–225.

Fontaine, A., Dubé, B., Malo, M., Ravenelle, J.F., Fournier, E., Mcnicoll, V., Beausoleil, C., Prud'homme, N., and Goutier, J, 2017. The Éléonore Gold Mine: Exploration, Discovery and Understanding of an Emerging Gold District in Eeyou Istchee James Bay, Superior Province, Northern Québec, Canada. "Proceedings of Exploration 17: Sixth Decennial International Conference on Mineral Exploration", paper 42.

Frimmel, H.E., 2008. Earth's continental crustal gold endowment. Earth and Planetary Science Letters, v.267, pp.45-55. https://doi.org/10.1016/j.epsl.2007.11.022.

Goldfarb, R.J., Groves, D.I., and Gardoll, S., 2001. Orogenic gold and geologic time: a global synthesis. Ore Geology Reviews,Volume 18, Issues 1–2, pages 1-75. https://doi.org/10.1016/S0169-1368(01)00016-6.

Goldfarb, R.J., and Groves, D.I., 2015. Orogenic gold: Common or evolving fluid and metal sources through time: Lithos, v. 233, p. 2–26, https:// doi.org/10.1016/j.lithos.2015.07.011.

Goldfarb, R.J., and Pitcairn, I., 2023. Orogenic gold: is a genetic association with magmatism realistic? *Miner Deposita* 58, pages 5–35. https://doi.org/10.1007/s00126-022-01146-8.

Goutier, J, et al. 2003. Synthese geologique de la region des lacs Sakami (33F) et Guyer (33G), Baie-James: Ministère des Ressources naturelles, Québec, Report DV 2002-12, p. 11−13.

Jochum, K.P., Willbold, M., Raczek, I., Stoll, B., and Herwig, K., 2005. Chemical characterization of the USGS reference glasses GSA-1G, GSC-1G, GSD-1G, GSE-1G, BCR-2G, BHVO-2G and BIR-1G using EPMA, ID-TIMS, ID-ICP-MS and LA-ICP-MS. Geostandards and Geoanalytical Research, v. 29, p. 285-302. https://doi.org/10.1111/j.1751- 908X.2005.tb00901.x.

Jochum, K.P., Weis, U., Stoll, B., Kuzmin, D., Yang, Q., Raczek, I., Jacob, D.E., Stracke, A., Birbaum, K., Frick, D.A., Günther, D., and Enzweiler, J., 2011, Determination of Reference Values for NIST SRM 610-617 Glasses Following ISO Guidelines. Geostandards and Geoanalytical Research, v. 35, no. 4, p. 397–429, doi: 10.1111/j.1751-908X.2011.00120.x.

Le Maitre, R.W., 1989. A Classification of Igneous Rocks and Glossary of Terms. Recommendations of the IUGS Commission on the Systematics of Igneous Rocks. Oxford: Blackwell.

Leventis, N.G., 2017. Exploring the source of metals in Archean orogenic gold deposits in the Abitibi Greenstone Belt, Canada. Masters Thesis, University of Stockholm.

Mercier-Langevin, P., Daigeneault, R., Goutier, J., Dion, C., and Archer, P., 2012. Geology of the Archean Intrusion-Hosted La-Grande-Sud Au-Cu Prospect, La Grande Subprovince, James Bay Region, Québec. Economic Geology (2012) 107 (5): 935–962, https://doi.org/10.2113/econgeo.107.5.935.

Niiranen, T., Lahti, I., and Nykänen, V., 2015. The orogenic gold potential of the central Lapland Greenstone Belt, northern Fennoscandian Shield, in Maier, W.D., et al., eds., Mineral Deposits of Finland: Amsterdam, Elsevier, p. 733–752, https:// doi.org/10.1016/B978-0-12-410438-9.00028-5.

Patten, C., Barnes, S., Mathez, E., and Jenner, F., 2013. Partition coefficients of chalcophile elements between sulfide and silicate melts and the early crystallization history of sulfide liquid: LA-ICP-MS analysis of MORB sulfide droplets. Chemical Geology, volume 358, pages 170-188, ISSN 0009-2541, https://doi.org/10.1016/j.chemgeo.2013.08.040.

Patten, C.G.C., Pitcairn, I.K., Teagle, D.A.H., and Harris, M., 2016a. Sulphide mineral evolution and metal mobility during alteration of the oceanic crust: Insights from ODP Hole 1256D.Geochimica et Cosmochimica Acta 193 (2016) 132–159.http://dx.doi.org/10.1016/j.gca.2016.08.009.

Patten, C.G.C., Pitcairn, I.K., Teagle, D.A.H., and Harris, M., 2016b. Mobility of Au and related elements during the hydrothermal alteration of the oceanic crust: implications for the sources of metals in VMS deposits. Min Dep 51, 179–200.

Patten, C.G.C., Pitcairn, I.K., Molnár, F., Kolb, J., Beaudoin, G., Guilmette, and C., Peillod, A., 2020. Gold mobilization during metamorphic devolatilization of Archean and Paleoproterozoic metavolcanic rocks. Geological Society of America, Geology, v.48. https://doi.org/10.1130/G47658.1

Patten, C. G. C., Molnár, F., Pitcairn, I. K., Kolb, J., Mertanen, S., and Hector, S., 2023. Multi-source and multi-stage metal mobilization during the tectonic evolution of the Central Lapland Greenstone Belt, Finland: implications for the formation of orogenic Au deposits. In Mineralium Deposita (Vol. 58, Issue 3, pp. 461–488). Springer Science and Business Media LLC. https://doi.org/10.1007/s00126-022-01133-z.

Peillod, A., 2019. Petrographic report. Stockholm University. Unpublish.

Percival, J.A., Skulski, T., Sanborn-Barrie, M., Stott, G.M., Leclair, A.D., Corkery, M.T., and Boily, M. 2012. Geology and tectonic evolution of the Superior Province, Canada. Chapter 6 In Tectonic Styles in Canada: The LITHOPROBE Perspective. Edited by J.A. Percival, F.A. Cook, and R.M. Clowes. Geological Association of Canada, Special Paper 49, pp. 321–378.

Phillips, G.N. and Powell, R., 2010. Formation of gold deposits-a metamorphic devolatilization model: Journal of Metamorphic Geology, v. 28, p. 689-718.

Piette-Lauzière, N., Guilmette, C., Bouvier, A., Perrouty, S., Pilote, P., Gaillard, N., Lypaczewski, P., Linnen, R.L., and Olivo, G.R., 2019. The timing of prograde metamorphism in the Pontiac subprovince, Superior craton: Implications for Archean geodynamics and gold mineralization: Precambrian Research, v. 320, p. 111–136, https://doi.org/10.1016/j.precamres.2018.10.016.

Pitcairn, I.K., Teagle, D.A.H., Craw, D., Olivo, G.R., Kerrich, R., and Brewer, T.S., 2006a. Sources of metals and fluids in orogenic gold deposits: Insights from the Otago and Alpine schists, New

Zealand: Economic Geology and the Bulletin of the Society of Economic Geologists, v. 101, p. 1525–1546, https://doi.org/10.2113/gsecongeo.101.8.1525.

Pitcairn, I.K., Warwick, P.E., Milton, J.A., and Teagle, D.A.H., 2006b. Method for ultra-low-lev analysis of gold in rocks: Analytical Chemistry, v. 78, p. 1290–1295, https://doi.org/10.1021/ ac051861z.

Pitcairn, I.K., Craw, D., and Teagle, D.A.H., 2015. Metabasalts as sources of metals in orogenic gold deposits: Mineralium Deposita, v. 50, p. 373–390, https://doi.org/10.1007/s00126-014-0547-y.

Pitcairn, I.K., Leventis, N., Beaudoin, G., Faure S., Dubé, B., 2017. A metasedimentary source of Au for the Abitibi? 15th Biennal SGA Conference, 20-23rd August 2017, Quebec, Canada.

Pitcairn, I. K., Clifford, P., Peillod, A., Guilmette, C., Gautier, J., and Beaudoin, G., 2019. Metabasalts as sources of gold in Archean greenstone belts. Conference paper: 15th Biennial SGA, Glasgow.

Pitcairn, I.K., et al., 2021. A metasedimentary source of gold in Archean orogenic gold deposits. Geology, v. 49, https://doi.org/10.1130/ G48587.1.

Ross and Bedard, 2009. Magmatic affinity of modern and ancient subalkaline volcanic rocks determined from trace-element discrimination diagrams. Canadian Journal of Earth Sciences, vol. 46, pp. 823-839.

Sappin, A.-A., Guilmette, C., Goutier, J., and Beaudoin, G., 2018. Geochemistry of Mesoarchean felsic to ultramafic volcanic rocks of the Lac Guyer area, La Grande Subprovince (Canada): Evidence for plume-related magmatism in a rift setting. Precambrian Research, v. 316, p. 83–102, https://doi.org/10.1016/j.precamres .2018.07.009.

Sylvester, P.J., Cabri, L.J., Tubrett, M.N., McMahon, G., Laflamme, J.H.G., and Peregoedova, A., 2005. Synthesis and evaluation of a fused pyrrhotite standard reference material for platinum group element and gold analysis by laser ablation-ICPMS: 10th International Platinum Symposium, , no. December 2015, p. 16–20.

Tomkins, A.G., 2010. Windows of metamorphic sulfur liberation in the crust: Implications for gold deposit genesis: Geochimica et Cosmochimica Acta, v. 74, p. 3246–3259, https://doi .org/10.1016/j.gca.2010.03.003.

Wilson, S.A., Ridley, W.I., and Koenig, A.E., 2002. Development of sulfide calibration standards for the laser ablation inductively-coupled plasma mass spectrometry technique: J. Anal. At. Spectrom., v. 17, no. 4, p. 406–409, doi: 10.1039/B108787H.

Websites:

GeoReM - Query by reference samples or materials (published values). http://georem.mpch-mainz.gwdg.de/sample_query.asp , May 4, 2024.